Chinese Journal of Chemical Engineering 94 (2026) 331–356

Contents lists available at ScienceDirect

Chinese Journal of Chemical Engineering

journal homepage: www.elsevier.com/locate/CJChE

Review

Engineering metal–organic framework architectures for enhanced carbon dioxide capture

Wanyi Zeng [1, 2], Minzhong Huang [3], Bin Chen [1, 2], Kok Bing Tan [1, 2], Dongren Cai [1, 2], Wanchai Pluempanupat [4], Guowu Zhan [1, 2, *]

[1] Academy of Advanced Carbon Conversion Technology, College of Chemical Engineering, Huaqiao University, Xiamen 361021, China
[2] Fujian Provincial Key Laboratory of Biomass Low-Carbon Conversion, Huaqiao University, Xiamen 361021, China
[3] Xiamen Institute of Rare Earth Materials, Haixi Institute, Chinese Academy of Sciences, Xiamen 361021, China
[4] Department of Chemistry and Center of Excellence for Innovation in Chemistry, Special Research Unit for Advanced Magnetic Resonance, Faculty of Science, Kasetsart University, Bangkok 10900, Thailand

ARTICLE INFO

Article history:
Received 28 September 2025
Received in revised form
2 December 2025
Accepted 25 December 2025
Available online 13 February 2026

Keywords:
Metal–organic frameworks
CO_2 capture
Adsorption
Nanomaterials
Surface modifications

ABSTRACT

The escalating concentration of atmospheric CO_2 is a major driver of global climate change, necessitating efficient capture technologies. Metal–organic frameworks (MOFs) have emerged as promising adsorbents due to their structural tunability, high surface areas, and porosity. However, their industrial deployment remains constrained by moderate adsorption capacities, limited stability under realistic conditions, selectivity challenges, and high production costs. This review systematically examines rational design strategies for enhancing MOF performance in CO_2 capture, integrating recent advances in material synthesis, characterization, and computational modeling. We discuss the role of theoretical approaches, including density functional theory, molecular simulations, and machine learning, in predicting adsorption behavior and guiding experimental efforts. Key optimization techniques explored encompass pore engineering, surface functionalization, metal site regulation, defect control, and composite formation. Furthermore, we evaluate selective adsorption mechanisms in complex gas mixtures and assess commercialization pathways, highlighting the importance of economic viability and sustainable synthesis methods. Finally, we outline future research directions aimed at improving cyclic stability, scalability, and industrial applicability, providing a cross-scale perspective on translating laboratory innovations into practical CO_2 capture applications.
© 2026 The Chemical Industry and Engineering Society of China, and Chemical Industry Press Co., Ltd. All rights are reserved, including those for text and data mining, AI training, and similar technologies.

1. Introduction

CO_2 is a critical contributor to the greenhouse effect, representing a significant challenge that demands a global resolution. The Intergovernmental Panel on Climate Change (IPCC) has established a mandate for nations to achieve carbon neutrality. Within this regulatory framework, carbon capture stands as a crucial and indispensable approach. Technologies for capturing CO_2 encompass amine-based solutions [1], amino adsorbents [2], zeolites [3], activated carbons [4], and metal–organic frameworks (MOFs).

Among them, MOFs, as solid adsorbents, are characterized by extensive surface areas, customizable pore sizes, and versatile designs, making them essential materials for CO_2 adsorption. MOFs integrating chemical functionalities with amino-functionalized MOFs form carbamate bonds with CO_2, enhancing both capacity [2] and DES@MOF-808 selectivity [5]. Furthermore, MOFs like CFA-Zn-OH utilize open metal sites for Lewis acid-base interactions, achieving adsorption enthalpies (-72 kJ·mol^{-1}) that surpass the physical adsorption limits of carbons [6]. MOFs offer a thermally benign alternative; materials like CALF-20 can be regenerated at 80 °C–120 °C, reducing energy demand by 30% to 50% while maintaining cyclic stability (>45000 cycles) [7]. The solid-state nature of MOFs also eliminates risks of solvent leakage and simplifies process integration, unlike liquid amine systems. Defect-engineered UiO-66 achieves a CO_2/N_2 selectivity of 49% *via* microwave-assisted synthesis [8,9].

This article is part of a special issue entitled: Sino-Thai Frontiers of Green Chemical Engineering published in Chinese Journal of Chemical Engineering.

* Corresponding author.
E-mail address: gwzhan@hqu.edu.cn (G. Zhan).

https://doi.org/10.1016/j.cjche.2025.12.040
1004-9541/© 2026 The Chemical Industry and Engineering Society of China, and Chemical Industry Press Co., Ltd. All rights are reserved, including those for text and data mining, AI training, and similar technologies.

Given the wide range of benefits associated with utilizing MOFs for CO_2 adsorption, they have attracted numerous researchers to focus on this area. For example, Zhao *et al.* [10] discussed the applications of MOFs across multiple domains, including carbon capture, energy storage, and environmental photocatalysis. Li *et al.* [11] addressed the development of MOF-based composite materials in CO_2 capture. They investigated the performance enhancements after the combination of MOFs with polymer membranes, gels, ionic liquids, *etc*., in addition to the challenges encountered in practical applications. While these reviews are excellent and should be read by aspiring researchers, given the expanding knowledge on CO_2 adsorption using MOF, some of these good reviews were published years ago, and hence, are not updated with current knowledge. Furthermore, the problems of low adsorption capacity, low selectivity, and insufficient stability of unmodified MOFs have not been systematically and thoroughly summarized in a classified manner in the above review.

Therefore, for this review, we will focus on the rational design and optimization strategies of MOFs as excellent adsorbents for CO_2, which includes recent studies. This review introduces the structural diversity of MOFs and analyzes the mechanisms of CO_2 adsorption by MOFs, innovatively integrating specific cases, quantitative characterization, and theoretical calculation comparisons to outline the correlation map of "structure-force-performance accurately". Notably, distinct from previous reviews [12], this work compares the strength differences of various interaction forces involved in CO_2 adsorption by MOFs, which is elaborated through combined characterization techniques and specific examples. When systematically reviewing strategies for enhancing CO_2 adsorption performance in MOFs, this review proposes the critical role of facet regulation in improving CO_2 adsorption capacity. Additionally, this review summarizes the composite mechanisms of MOFs with porous carbon, polymers, ionic liquids, and other materials. Breaking through the limitations of traditional reviews, pilot-scale and above data were innovatively incorporated to deduce scientific problems from an industrial perspective and validate solutions with case studies, thereby bridging the gap from "laboratory innovation" to "engineering implementation" for researchers. Finally, the review will discuss the future and outlook for the development of MOFs in CO_2 capture. It is sincerely hoped that this review will provide an excellent guideline for future researchers interested in this field.

2. Representative MOFs for CO_2 Capture

Classification of typical CO_2 capture MOFs falls into several categories based on distinct uptake mechanisms. These range from frameworks leveraging open metal sites (*e.g*., MOF-74) for Lewis acid-base interactions and flexible structures (*e.g*., MILs) demonstrating gate-opening, to highly stable frameworks (*e.g*., UiO-66, CALF-20) and zeolitic imidazolate frameworks (ZIFs). Furthermore, functionalization with groups like amines or integration into composites bolsters their performance, even in challenging environments, highlighting their significant potential for industrial CO_2 separation. The following sections will detail these representative MOFs.

2.1. MOF-74

MOF-74, also referred to as M_2(dihydroxy terephthalic acid), or M_2(DHTP) or CPO-27, is a three-dimensional lattice framework synthesized from metals, including Mn, Co, Fe, Ni, and Mg, Cu, Zn, coordinated with 2,5-dihydroxy terephthalate ligands [13]. There are high-density open metal sites at the corners of the hexagonal pores. By removing the coordinating molecules, Lewis acid sites with strong affinity for CO_2 can be generated. Among MOFs with open metal sites, Mg-MOF-74 has a higher CO_2 adsorption capacity than other transition metal-based MOF-74. The reason is that the interaction strength between the open sites of Mg^{2+} and CO_2 is significantly higher than that of most other metal sites. In the Mg_2(dobdc) series of MOF-74, the CO_2 adsorption enthalpy ($-Q_{st}$) of Mg_2(dobdc) is approximately 44 kJ·mol^{-1}, while that of other metals, such as Ni^{2+} (39 kJ·mol^{-1}) and Fe^{2+} (33 kJ·mol^{-1}) [13]. This indicates that the open sites of Mg^{2+} have a stronger affinity for CO_2. The Lewis acidity of Mg^{2+} is significantly stronger than that of most transition metal ions. As a main group metal ion, Mg^{2+} has a small ionic radius (about 0.072 nm) and a high charge density (charge/volume ratio), thus exerting a stronger electrostatic attraction on the quadrupole moment of CO_2 (a polar molecule with a quadrupole moment). Transition metals (such as Zn^{2+}) have a larger ionic radius, resulting in weaker electrostatic interaction with CO_2. Fig. 1(a) shows types of metal sources and ligands for MOF-74 [13]. Fig. 1(b) shows a schematic diagram of the preparation process of traditional Mg-MOF-74. The metal source $Mg(NO_3)_2 \cdot 6H_2O$ and the organic ligand 2,5-dihydroxy terephthalic acid were dissolved in a solvent system, which underwent a solvothermal reaction, and three-dimensional microporous crystals were formed. Subsequently, the solvent was replaced with methanol, and the crystals were activated by vacuum heating. This activation process removed the DMF/H_2O molecules that occupied the sixth coordination site of Mg^{2+}, ultimately yielding the traditional Mg-MOF-74 with open metal sites [14].

2.2. ZIFs

ZIFs constitute a distinctive class of MOF materials characterized by a tetrahedral three-dimensional network structure analogous to that of zeolites. In ZIFs, zinc or cobalt serves as a substitute for silicon found in zeolites, while imidazole ligands replace the oxygen bridges typical of zeolitic structures. In 2006, the Yaghi group [15] documented the structural composition of ZIF-1 through ZIF-12. Following this, in 2007, the group described ZIF-20 to ZIF-23, recognizing their application in CO_2 adsorption [16]. In 2008, the Yaghi group [17,18] reported additional structures, including ZIF-68, ZIF-69, ZIF-70, ZIF-95, and ZIF-100, marking a significant expansion of the ZIF-based MOFs. Through modifications in the synthesis process and crystallization conditions, it is possible to obtain ZIF materials sharing identical compositions but exhibiting entirely different topological structures. A prominent example, ZIF-8, features primary pore diameters of 1.16 nm and secondary pore diameters of 0.34 nm. The adjustable pore dimensions and chemical properties of ZIF materials can be tailored by altering the organic ligands or metal centers, thereby optimizing the adsorption efficacy for specific gases. Banerjee *et al.* [19] synthesized various ZIF materials employing zinc nitrate, 2-nitroimidazole, and combinations of differently functionalized imidazoles, achieving variations in pore sizes through ligand modifications. Fig. 2(a) illustrates the structural configurations of ZIF-68 through ZIF-81 [19].

ZIFs (including ZIF-68–81) all contain 2-nitroimidazole (nIm), which is fixedly located at the edges of hpr cages, forming a stable framework. ZIF-68–81 also includes a second type of ligand, which are substituted imidazoles (such as –Cl, –CN, –Me, –Br, –NO_2, *etc.*). These ligands determine the pore size (0.71–1.59 nm) and surface polarity, thereby affecting CO_2 adsorption selectivity. In the ZIFs series, ZIF-78 (Zn), containing the –NO_2 group, exhibits higher CO_2 capture capacity and CO_2/N_2, CO_2/CH_4 selectivities compared to isostructural ZIFs containing other functional groups such as –CN and –Br, due to the dipole–quadrupole interactions [19]. ZIF-8 is a typical ZIF material. Fig. 2(b) shows the overall

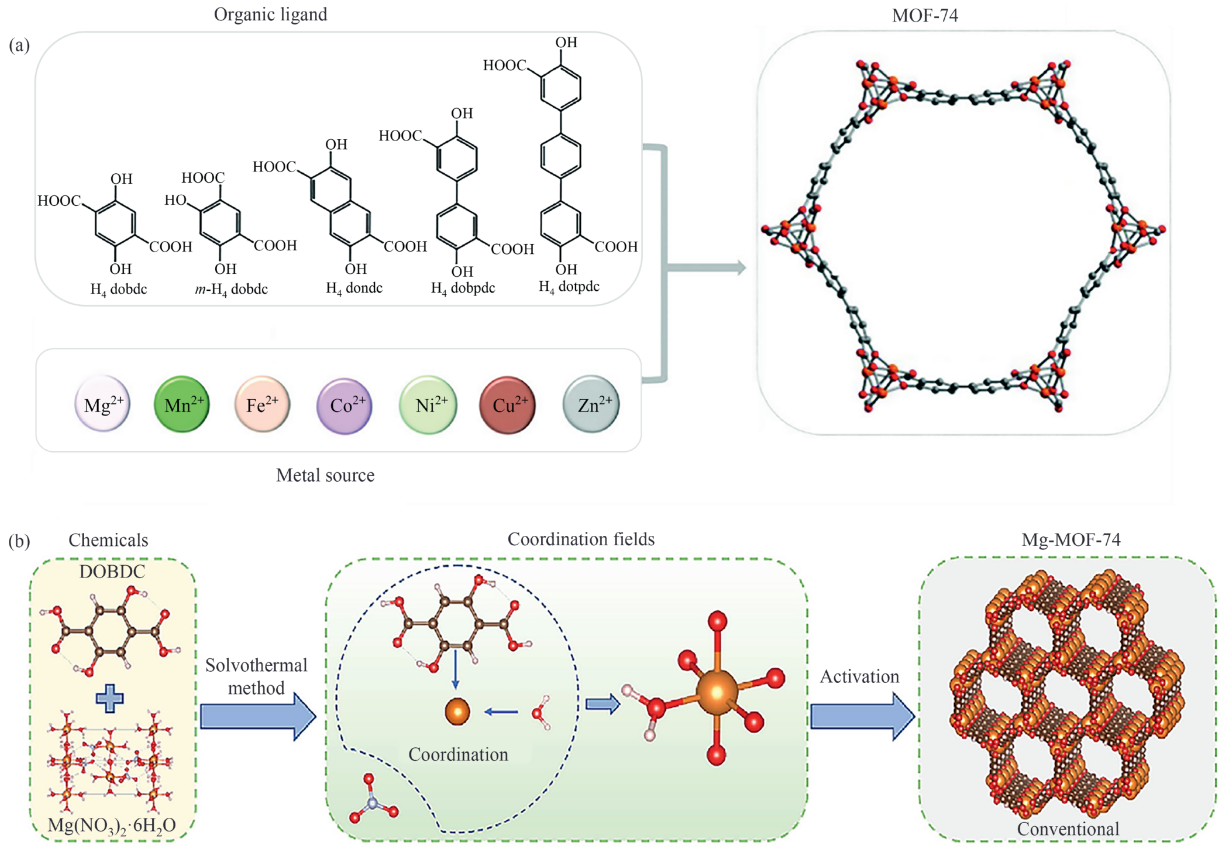


Fig. 1. (a) Types of metal sources and organic ligands for MOF-74 [13], reprinted with permission from Choe *et al.*, Copyright 2021, Royal Society of Chemistry. (b) Schematic diagram of the preparation process of traditional Mg-MOF-74 [14], reprinted with permission from An *et al.*, Copyright 2023, Elsevier B.V.

connection mode of the ZIF-8 framework, presenting its typical sodalite topology, which is formed by the interconnection of multiple secondary structural units (ZnN_4 tetrahedra and imidazole rings) to create a 3D interconnected pore cage network. Fig. 2(c) is the ZIF-8 unit cell for GCMC simulation, showing that the basic structural unit of ZIF-8 used in the simulation is a cubic unit cell, with the unit cell edge length labeled as 1.6991 nm and the boundary of the $1 \times 1 \times 1$ unit cell marked with a solid line. Fig. 2(d) shows the synthesized ZIF-8 crystals exhibit a regular rhombic dodecahedral shape [20].

2.3. MILs

MIL series materials, named after the Material Institute Lavoisier, are highly esteemed for their unique porous structures and large specific surface areas, making them particularly suitable for gas adsorption applications [21,22]. The synthesis of MIL materials typically involves the use of lanthanide and transition metals in combination with dibasic carboxylic acids (such as glutaric acid and succinic acid). Additionally, trivalent metals (such as Cr, Fe, Al, V, Ga, and In) can be used in conjunction with carboxylic acids like terephthalic acid or trimesic acid [23]. Dynamically flexible MOFs are a class of nanoporous materials with unique structural responsiveness. Their core characteristic is that the pore structure can undergo reversible contraction and expansion, known as the "breathing effect", in response to external conditions(such as gas molecule adsorption and pressure changes) [23]. MIL-53 (containing Al^{3+} or Cr^{3+}) has hydroxyl (μ_2-OH) groups in its structure. During the CO_2 adsorption process, CO_2 molecules interact specifically with hydroxyl groups in the initial stage, leading to the contraction of the pore structure. As the pressure increases, the pores reopen, and complete pore filling occurs. This reversible structural change enables it to exhibit a unique stepwise adsorption behavior for CO_2 [24]. Fig. 3(a), (b) shows the respiratory effect of MOF, demonstrating the hydration and dehydration process of MIL-53 (Al, Cr). Fig. 3(a) shows the hydrated state ($MIL\text{-}53_l$), at which point the pore is slightly deformed due to hydrogen bonding between water molecules and carboxylate oxygen atoms and μ_2 hydroxyl groups; Fig. 3(b) shows the dehydrated state ($MIL\text{-}53_h$), and after heating to remove water, the structure transforms into a more open porous form. Fig. 3(c), (d) shows the adsorption isotherm of CO_2 and CH_4 on MIL-53 (Al) and MIL-53 (Cr), respectively. The CO_2 adsorption curves exhibit a "step" phenomenon, while the CH_4 adsorption curves are smooth. The step phenomenon in the CO_2 adsorption curves of MIL materials is related to the permanent quadrupole moment of CO_2. CO_2 has specific interactions with the hydroxyl groups of the MIL-53 material, whereas CH_4, lacking a quadrupole moment, does not produce the step effect. This step may result from the "breathing effect" (structural change) of MIL-53. For instance, in the initial stage, the interaction between CO_2 and hydroxyl groups leads to structural shrinkage; as the pressure increases, the pores reopen to complete the overall filling (similar to the structural transition during water adsorption).

In contrast, MIL-47 does not have the breathing effect, and its CO_2 adsorption isotherms show no obvious steps, which further confirms the correlation between the breathing effect and the hydroxyl groups in the structure as well as the quadrupole moment interaction of guest molecules. In the field of gas separation, the selective adsorption capacity of MIL-53 for CO_2 (due to

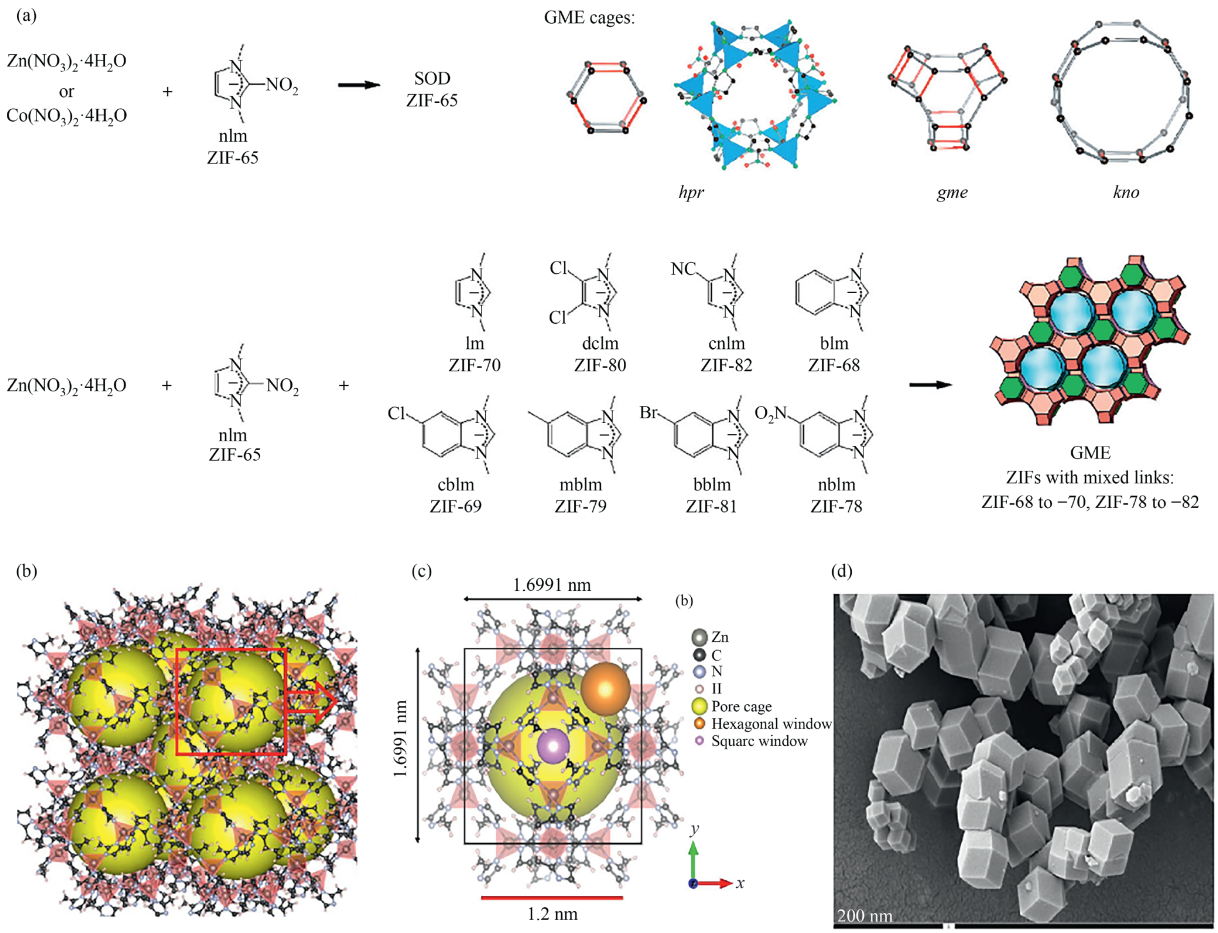


Fig. 2. (a) The synthetic routes and structures of ZIFs [19], reprinted with permission from Banerjee *et al.*, Copyright 2009, American Chemical Society. (b) The sodalite topology of ZIF-8, (c) the ZIF-8 unit cell for GCMC simulation, (d) SEM image of ZIF-8 [20] is an open-access article without the requirement to obtain permission.

the stronger interaction between the quadrupole moment of CO_2 and the framework, while CH_4 does not have this characteristic) can be used for the separation and purification of CO_2 and CH_4 in natural gas. The CO_2 adsorption capacity reaches 10 mmol·g^{-1} at 3 MPa, significantly exceeding that of traditional zeolites, indicating high efficiency and separation potential. In terms of gas storage, the reversible pore structure changes brought about by the breathing effect help optimize the gas adsorption–desorption efficiency.

The core structure of MIL-101 is a hierarchical porous network constructed by metal-oxygen clusters (Cr/Al/Fe) and 1,4-benzenedicarboxylic acid (BDC) ligands, which simultaneously possesses a high specific surface area, open metal sites, and tunable pores. The secondary building unit (SBU) of MIL-101 (Cr) is a $Cr_3(OH/F)$ trimer, where one Cr atom coordinates with F or OH groups, and the other two Cr atoms are unsaturated metal sites providing Lewis acid sites for adsorption. As shown in Fig. 4(a) and (b), MIL-100 (Cr) uses 1,3,5-benzenetricarboxylic acid (BTC) as the ligand, which is a tritopic linker, meaning one ligand molecule can connect three metal nodes; the ligand of MIL-101 (Cr) is BDC, a ditopic linker that connects two metal nodes per ligand molecule. This difference in linker connectivity results in a stronger interconnection between the metal nodes of MIL-100(Cr). As shown in Fig. 4(c) and (d), the mechanical stability of MIL-100(Cr) is significantly superior to that of MIL-101(Cr), due to that its tritopic linker (BTC) has higher connectivity than the ditopic linker [25].

2.4. UiO-66

The strength of coordination bonds formed between metal ions and organic ligands is critical to the stability of MOFs. Metal ions with small ionic radii and high charges (such as Zr and Hf) form strong coordination bonds, endowing materials with excellent thermal stability. Highly stable MOFs are represented by UiO-66. UiO-66 is usually synthesized from tetravalent zirconium ions (Zr^{4+}) and BDC ligands. The Zr^{4+} ions, with a small radius and high charge, form strong coordinate bonds with the ligands, endowing them with excellent chemical and thermal stability. UiO-66 is a typical representative of this type of MOF. By selecting different tetravalent metal sources, such as Zr^{4+}, Hf^{4+}, and Ce^{4+}, a variety of UiO-66 series MOF materials can be prepared. UiO-66, an acronym denoting the University of Oslo, is commonly synthesized using tetravalent zirconium ions together with BDC ligands [26]. Fig. 5(a)–(d) shows the structure of UiO.

UiO-66 demonstrates high hydrothermal stability, structural robustness, and tunability, retaining its framework even under defective conditions. The type and location of defects have a significant influence on CO_2 adsorption behavior. Two defect types are considered. In Defect 1, Fig. 5(e)–a terephthalic acid (BDC) linker is missing from a Zr_6 cluster node and replaced by four –OH groups. In Defect 2, Fig. 5(f)–a linker is similarly substituted but at a non-corner site, closer to the cavity center. This positional difference alters the selectivity of CO_2 and water [27].

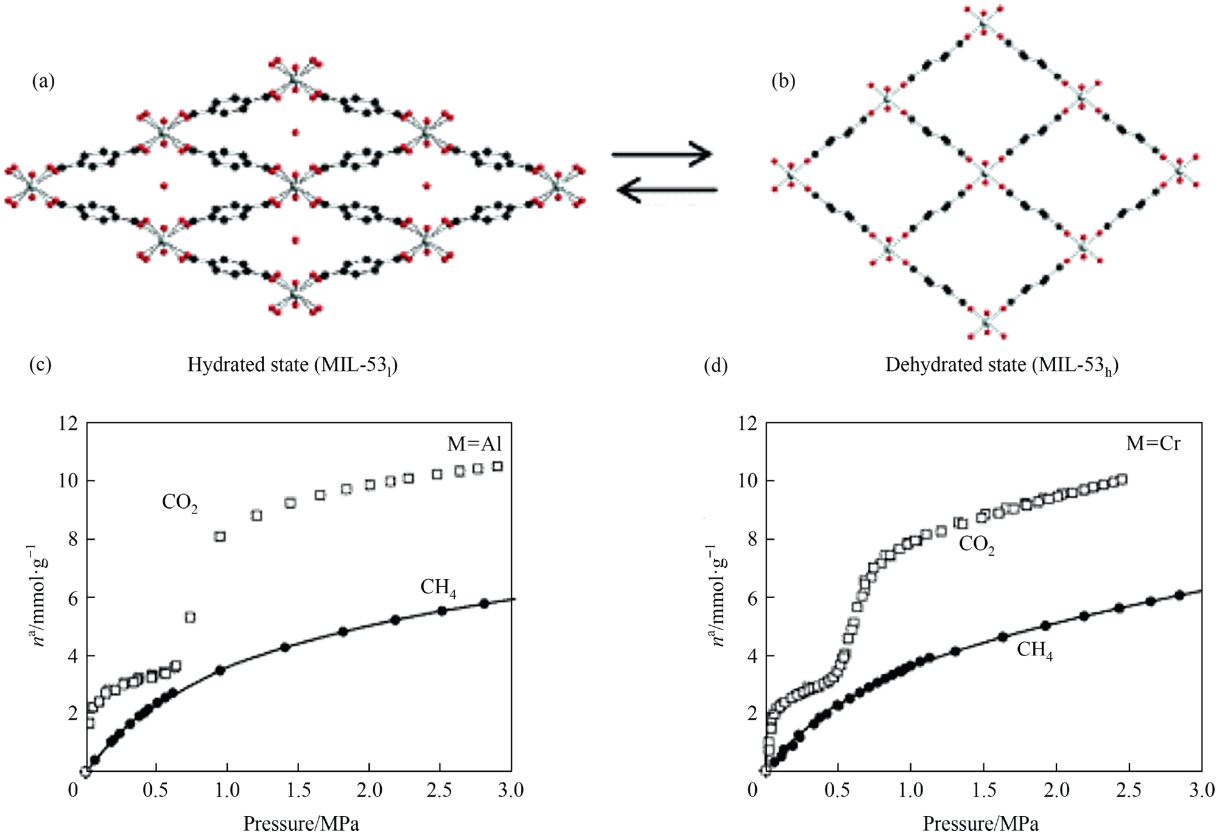


Fig. 3. (a), (b) The hydration and dehydration of MIL-53 (Al, Cr). (c), (d) The adsorption isotherm of CO_2 and CH_4 on MIL-53 (Al) and MIL-53 (Cr) [24]. Reprinted with permission from Bourrelly *et al.*, Copyright 2005, American Chemical Society.

2.5. CALF-20

CALF-20, the full name of which is Calgary Framework 20, is a scalable MOF material developed by a team led by G.K.H. Shimizu from the University of Calgary in Canada [7]. It can serve as a long-lasting physical adsorbent for CO_2 capture. CALF-20 not only has a high physical adsorption capacity for CO_2 but also shows a certain selectivity for water [7]. In terms of structure, CALF-20 has a three-dimensional framework structure, and its basic structural unit is the zinc-triazole layer. Specifically, 1,2,4-triazole forms a two-dimensional layer by bridging zinc ions, and oxalate ions act as struts to connect these two-dimensional layers, ultimately forming a topological structure [28]. Fig. 6(a) shows a 3D schematic diagram of CALF-20's structure, and Fig. 6(b) shows a simplified schematic diagram of CALF-20's topological structure [28].

α-CALF-20 has a chemical formula of $[Zn_2(ox)(trz)_2]\cdot s$, where "s" denotes solvent molecules. In this phase, Zn^{2+} ions are five-coordinated, with a coordination environment composed of three nitrogen atoms from trz ligands and one oxygen atom from an ox ligand, resulting in a distorted trigonal bipyramidal geometry. CALF-20, $[Zn_2(ox)(trz)_2]$, undergoes fully reversible humidity-driven α→β single-crystal-to-single-crystal transitions (≥23% RH) [29], and temperature-driven α→τ→γ sequences (80 °C, 7–10 days), yielding four polymorphs with distinct Zn coordination: α (5-coordination, trigonal bipyramidal), β (4-coordination), τ (5- and 6-coordination with Ow (oxygen atom of a coordinated water molecule), Zn–Ow 0.2497 nm), and γ (5- and 6-coordination, Zn–Ow 0.2320 nm, 9% unit-cell contraction). The triazolate ligand confers robust water and acid stability. α-CALF-20 exhibits the highest CO_2 capacity; CO_2 adsorption (1 MPa) forms $[Zn_2(ox)(trz)_2]\cdot CO_2$ while preserving the α framework [30]. At 40% RH, CO_2 remains preferentially adsorbed, with water hydrogen-bonded within the pores. After 45000 steam cycles, the adsorption performance remains 98% [7].

2.6. HKUST-1

HKUST-1 is formed by the connection of triangular BTC. Cu^{2+} tends to create open sites due to the Jahn–Teller effect [31]. The Jahn–Teller effect is related to the formation of open metal sites in HKUST-1. Specifically, for Cu^{2+}, as a configuration ion, the Jahn–Teller effect causes the ligands to form longer M–L bonds with weaker bonding forces. It tends to create a square planar geometry. This effect facilitates the removal of coordinated water molecules from Cu^{2+}, thereby forming open metal sites during the activation process. These sites, acting as Lewis acid centers, can interact strongly with CO_2, which in turn affects the CO_2 adsorption performance of HKUST-1. In simple terms, the Jahn-Teller effect manifests here as the distortion of the coordination environment of Cu^{2+} due to the asymmetry of its electronic configuration, favoring the formation of open metal sites [32].

2.7. Anion pillared MOFs

Anion pillared metal–organic frameworks (APMOFs) represent a distinct category of porous materials constructed by incorporating inorganic anion pillars (*e.g.*, MF_6^{2-}, $MO_xF_{6-x}^{2-}$, $Cr_2O_7^{2-}$, *etc.*) into the scaffold of traditional MOFs. These pillars not only serve as structural supports but also provide abundant hydrogen-bond acceptors (*e.g.*, F, O), enabling strong host–guest interactions. APMOFs typically consist of three synergistic components: (1) Metal nodes, often transition metal ions (*e.g.*, Cu^{2+}, Ni^{2+}, Zn^{2+},

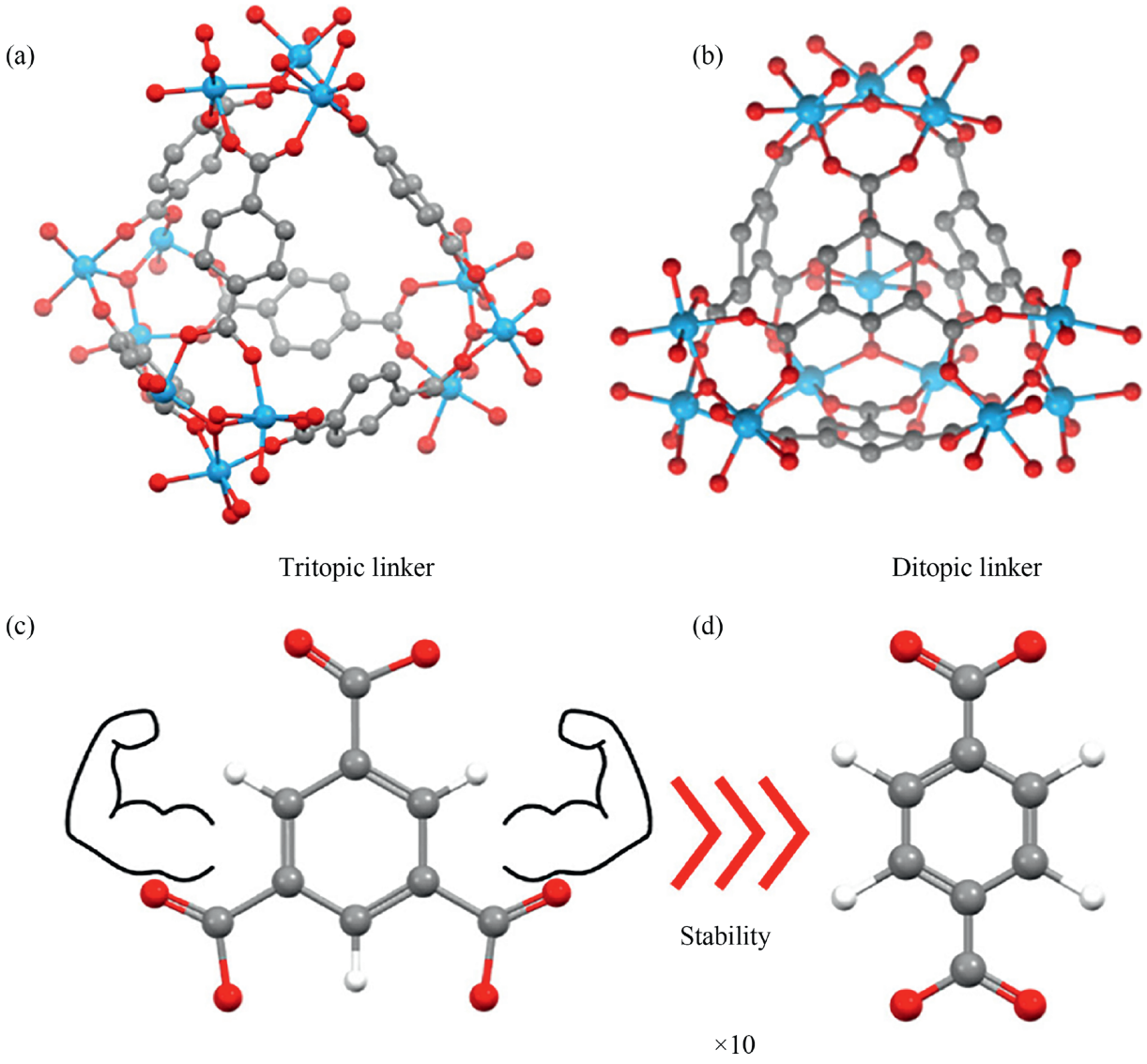


Fig. 4. The architectural framework of (a) MIL-101(Cr), (b) MIL-100(Cr). The ligand of (c) MIL-101(Cr), (d) MIL-100(Cr) [25]. Reprinted with permission from Celeste *et al.*, Copyright 2024, American Chemical Society.

Co^{2+}), forming the basis of two-dimensional layered structures. (2) Organic ligands, primarily N-donor linkers (*e.g.*, bipyridine, pyrazine), which define the channel dimensions and functional sites. (3) Anion pillars, which cross-link the metal-ligand layers into stable three-dimensional frameworks while providing strong electrostatic binding sites for gas molecules.

Notable examples of APMOFs include SIFSIX-3, ZU-66 (ZrFSIX-2-Zn-*i*), and ZNU-1 (BSF-9-Cu) [33]. For instance, ZU-66 is constructed from 4,4′-bipyridylacetylene, Zn^{2+} nodes, and ZrF_6^{2-} pillars. It exhibits a doubly interpenetrated PCU topology with pore apertures ranging from 0.355 to 0.501 nm. The restricted 0.355 nm channel enables molecular sieving of CO_2 (0.33 nm) over CH_4 (0.38 nm) and N_2 (0.365 nm). CO_2 molecules interact with ZrF_6^{2-} pillars *via* electrostatic interactions (0.276 nm) and van der Waals contacts (0.266–0.291 nm), adopting a tilted orientation (40.4°) for optimal binding [34]. SIFSIX-3 is formed by the linkage of divalent metals with pyrazine ligands [35]. Among the SIFSIX-3 series, SIFSIX-3-Cu has the largest isosteric heat of adsorption (Q_{st}) for CO_2 and relatively strong adsorption capacity. The order of CO_2 Q_{st} values is as follows: SIFSIX-3-Cu > SIFSIX-3-Ni > SIFSIX-3-Co > SIFSIX-3-Zn > SIFSIX-3-Fe. Due to the Jahn–Teller effect, the crystal structure of SIFSIX-3-Cu exhibits a smaller pore size and shorter *a*/*b* unit cell length, resulting in differences in the radial distribution function and dipole distribution of CO_2 adsorption compared to other analogues, which in turn affect its CO_2 adsorption performance [35].

2.8. MOF-5

MOF-5, represented by the chemical formula $Zn_4O(BDC)_3$, constitutes a MOF characterized by cubic symmetry. This crystalline structure remains stable even when desolvated and heated up to 300 °C. Within the structure of MOF-5, each metal node comprises a Zn_4O cluster, consisting of four Zn^{2+} and four oxygen atoms. Each Zn_4O cluster is linked to three BDC ligands, which coordinate with the metal node through their carboxylate groups. The crystal structure of MOF-5 maintains a degree of stability; however, structural integrity may be compromised during the compaction process. Fig. 7 illustrates the growth of MOF-5 crystals across different crystallographic facets [36].

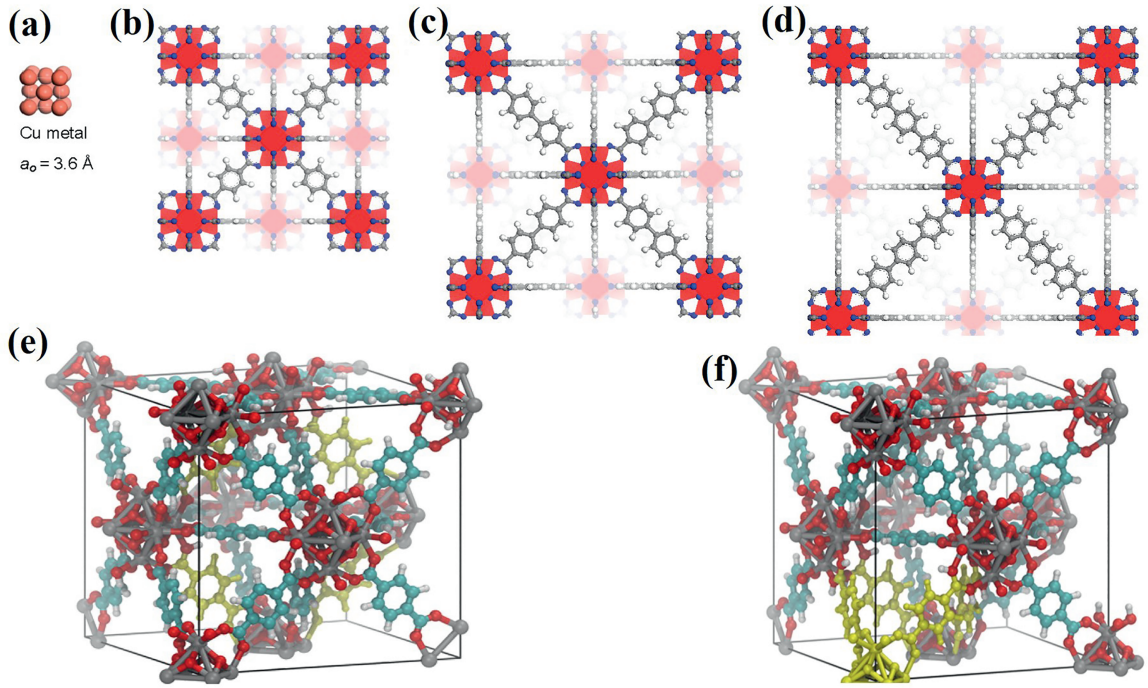


Fig. 5. (a) Single copper unit cell; (b) UiO-66, a Zr-MOF employing 1,4-benzene-dicarboxylate (BDC) as its linker; (c) UiO-67, a Zr-MOF employing 4,4′-biphenyl-dicarboxylate (BPDC) as its linker; and (d) UiO-68, a Zr-MOF employing terphenyl-dicarboxylate (TPDC) as its linker [26]. Reprinted with permission from Cavka *et al.*, Copyright 2008, American Chemical Society. (e) Defect-1 of UiO-66; (f) defect-2 of UiO-66 [27]. Reprinted with permission from Ma *et al.*, Copyright 2019 Elsevier Ltd.

2.9. Comparisons of CO_2 adsorption capacity

In addition to the typical MOFs introduced above, numerous other MOF materials can also be utilized for CO_2 adsorption [37]. Table 1 presents the CO_2 adsorption capacities of various MOFs. As can be seen, CALF-20 (Zn-triazole) achieves water resistance and cyclic stability (>45000 cycles) through humidity-responsive phase transformation [7], whereas the MIL series (Al/Cr) demonstrates weak stability in acidic environments. HKUST-1 showcases the highest adsorption capacity (11.6 mmol·g^{-1}) [52], followed by Mg-MOF-74 (10.04 mmol·g^{-1}) [51]. In comparison, MIL-101(Cr) (1.81 mmol·g^{-1}) [39] exhibits relatively lower capacities, reflecting the decisive influence of metal centers and ligand structures on adsorption performance.

3. Adsorption Mechanism of MOFs for CO_2 Capture

MOFs capture CO_2 *via* a combination of physical and chemical adsorption processes. The interaction of weak, non-covalent forces, including van der Waals forces, dipole–dipole interactions, π–π stacking, π–quadrupole interactions, and hydrogen bonding, characterizes physical adsorption. In contrast, chemical adsorption is distinguished by the formation of new chemical bonds. These two adsorption mechanisms will be further elaborated in the subsequent sub-sections.

3.1. Physical adsorption

In MOFs, physical adsorption encompasses various non-covalent interactions, including van der Waals forces, π–quadrupole, electrostatic interactions, dipole–dipole interactions, and hydrogen bonding. This form of adsorption typically refers to the adherence of CO_2 molecules to the inner surfaces of pores within MOFs. This process is intrinsically linked to the pore architecture and specific surface area of the MOFs [57,58]. van der Waals forces, though relatively weak, play a crucial role in the

Table 1
CO_2 adsorption capacities of MOF-based materials.

Material name	Condition	Adsorption capacity/mmol·g^{-1}	Reference
Ce-UiO-66	273 K, 0.1 MPa	2.53	[40]
Zr-UiO-66	273 K, 0.1 MPa	3.02	[9]
UiO-66(Zr)-$(OH)_2$	298 K, 0.1 MPa	6.23	[41]
ZIF-67@HCS-40	273 K, 0.1 MPa	4.60	[42]
Mg-MOF-74	298 K, 0.1 MPa	7.38	[27]
Mg-MOF-74	273 K, 0.1 MPa	6.80	[14]
Mg-MOF-74	298 K, 0.1 MPa	6.00	[14]
Defect Mg-MOF-74	273 K, 0.1 MPa	7.80	[14]
Defect Mg-MOF-74	298 K, 0.1 MPa	7.10	[14]
UiO-66-SO_3H-NH_2	298 K, 0.1 MPa	2.17	[43]
Zr-UiO-66	298 K, 0.1 MPa	1.11	[44]
UiO-66-NH_2 aerogel	298 K, 0.1 MPa	2.13	[45]
NH_2-UiO-66	298 K, 0.1 MPa	3.32	[46]
NH_2-$Cu_3(BTC)_2$	298 K, 0.1 MPa	3.86	[46]
30TEPA/UiO-66	348 K, 0.1 MPa	3.70	[47]
25TETA/UiO-66	298 K, 0.1 MPa	1.56	[44]
Ethlyenediamine@UiO-66	298 K, 0.1 MPa	3.48	[48]
B-ZIF-7(NO_3)	300 K, 0.1 MPa	2.20	[38]
MIL-101(Cr)	298 K, 0.1 MPa	1.81	[39]
DES@UiO-66-COOH	298 K, 0.1 MPa	2.1	[49]
NH_2-MIL-101(Cr)	298 K, 0.1 MPa	1.90	[21]
NH_2-MIL-53(Al)	303 K, 0.1 MPa	2.30	[50]
Mg-MOF-74	273 K, 0.1 MPa	10.04	[51]
HKUST-1	273 K, 0.1 MPa	11.6	[52]
Mg-MOF-8NH_2	303 K, 0.1 MPa	3.90	[53]
Zn-MOF-74	273 K, 0.1 MPa	2.46	[54]
COK-17	298 K, 0.1 MPa	2.50	[55]
CALF-20	293 K, 0.12 MPa	4.07	[7]
MOF-74(Ni)	273 K, 0.1 MPa	8.29	[56]

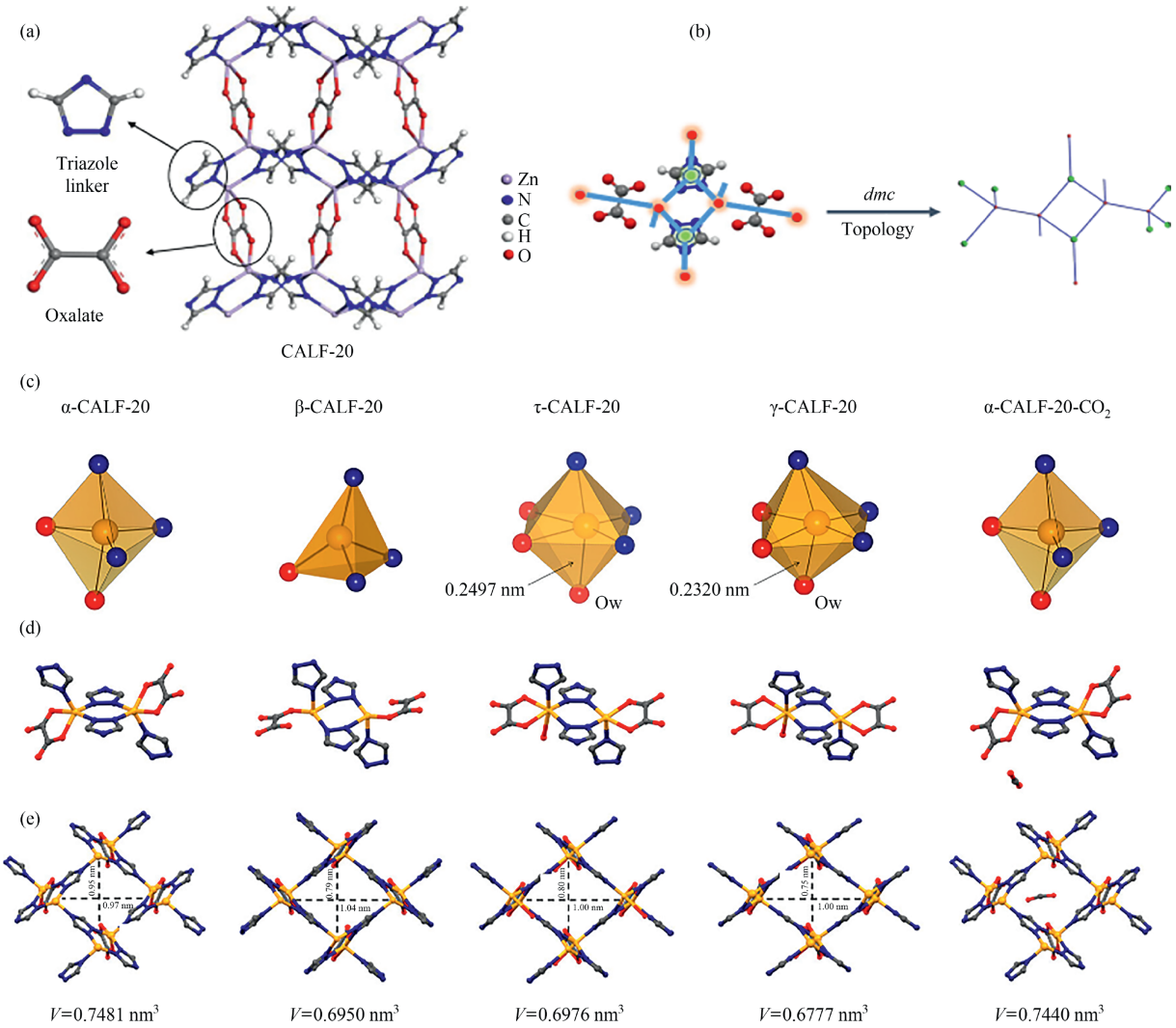


Fig. 6. (a) 3D structure diagram of CALF-20, (b) a simplified topological structure of CALF-20 [28]. Reprinted with permission from Oktavian *et al.*, [28] is an open-access article, Copyright 2024. (c)–(e) Structural diagrams of several CALF-20 phases [30]. Reprinted with permission from Drwęska *et al.*, Copyright 2024, American Chemical Society.

mechanism of physical adsorption of CO_2. van der Waals forces constitute the dominant driving force for CO_2 physisorption, which can't be directly "observed" by any single instrument, their existence is unambiguously inferred through an ensemble of indirect descriptors—namely, (i) the isosteric heat of adsorption, (ii) the temperature-dependent shape of adsorption isotherms, and (iii) textural metrics such as BET surface area and micropore volume. Due to their weak, non-specific nature, processes controlled by van der Waals forces exhibit low heats of adsorption (typically 20–40 kJ·mol^{-1}). Application of the Clausius–Clapeyron equation to CO_2 isotherms measured at 288, 298, and 313 K yields an isosteric heat of only 21 kJ·mol^{-1} for pristine MIL-101-Cr (Fig. 8(a)) [39]. Centrum voor Oppervlak techemie en Katalyse-17 (COK-17 is a new type of flexible zeolitic-imidazolate framework Zn(4,5-dichloroimidazolate)$_2$) enhances CO_2 adsorption by augmenting the London dispersion force imparted by chlorine substitutions in the imidazolate link. DFT calculations on COK-17 afford adsorption energies of −28 and −31 kJ·mol^{-1} (Fig. 8(b)). By means of Rietveld refinement of X-ray diffraction (XRD) data, the adsorption sites and packing configurations of CO_2 within the pores of COK-17 were determined [55]. The pronounced negative temperature coefficient of capacity further validates the physisorption fingerprint. At 0.1 MPa, the CO_2 uptake of MIL-101-Cr decreases monotonically from 288 K to 298 K to 313 K, a behavior that mirrors the exothermic character of van der Waals forces interactions and is fully consistent with the van't Hoff relationship [39].

Ma *et al.* [27] employed the Kamlet–Taft method to determine the solvent polarity parameter (β/α value, which reflects the balance of hydrogen bond-donating/accepting capabilities of the solvent) to study the performance of Mg-MOF-74. Specifically, the β/α value controls the balance between crystal nucleation and growth by influencing the deprotonation rate of 2,5-dihydroxyterephthalic acid; it affects the coordination strength and thermal stability by altering the coordination environment of Mg^{2+}. The linear correlation between the BET area (Fig. 8(c)) and CO_2 capacity quantitatively links uptake to the density of van der Waals forces-accessible sites. In contrast, post-synthetic modification reduces the surface area and therefore attenuates the contribution of van der Waals forces. The combination of (i) high BET area (Fig. 8(c)), (ii) reversible type-I isotherm, and (iii) facile regeneration over multiple cycles (low regeneration energy consumption and high-frequency cycles) (Fig. 8(d)) provides

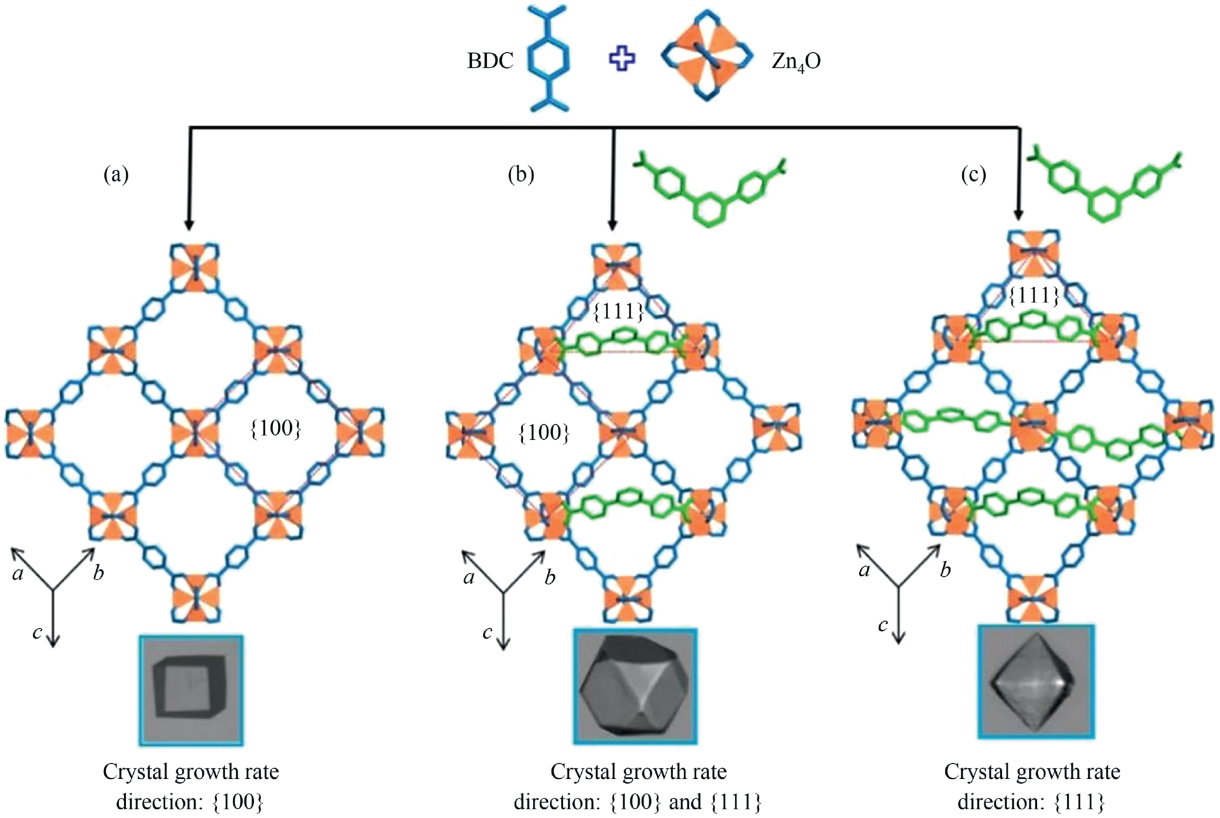


Fig. 7. The development of MOF-5 crystals on various crystallographic facets [36]. Reprinted with permission from Suresh *et al.*, Copyright 2021, American Chemical Society.

compelling indirect evidence for van der Waals forces dominance [27]. In Mg-MOF-74, this weak dispersive manifold cooperates with stronger Mg–O coordinative interactions to dictate overall CO_2 adsorption performance [27].

Meanwhile, π–quadrupole stacking interactions are of notable significance between π–electron systems and are particularly important for the interaction of aromatic rings within MOFs. These π–π stacking interactions in MOFs are facilitated by collective charge fluctuations, which exhibit non-local and cooperative characteristics. Li *et al.* [59] conducted first-principles theoretical calculations to investigate the adsorption forces of CO_2 on the (100) and (010) facets of MOFs. Their findings indicated that π–π interactions, involving the benzene ring surface, predominate in CO_2 binding on the 100 facets. Conversely, dispersion forces primarily mediate CO_2 interactions on the (010) facets [59]. DFT (VASP, PW91-D2) calculations were employed to determine the CO_2 adsorption energies, optimize structures, and perform charge analysis on different crystal facets, confirming the dominance of dispersion interactions. BET model fitting of experimental data yielded an adsorption energy of 0.32 eV, which is close to the DFT-calculated value of 0.25 eV, thereby validating the reliability of the computational approach [59]. CO_2 molecules engage in quadrupole–π electron interactions with imidazolate rings within the ZIF-8 framework. The electron-donating nature of the amino group enhances the interaction between the quadrupole moment of CO_2 and the π–electrons of imidazolate rings in ZIF-8, considerably augmenting CO_2 adsorption [60]. Dipole–quadrupole interaction is also one of the forces for CO_2 adsorption. The $-NO_2$ group mainly interacts with CO_2 through dipole-quadrupole interaction, and in addition, the C–H bonds on adjacent aromatic rings are polarized due to the electron-withdrawing effect of $-NO_2$, thereby forming hydrogen bonds with the O atoms of CO_2 [19].

Electrostatic interactions occur between charged particles or polar molecules, with their magnitude dependent on charge distribution and intermolecular distance. Electrostatic interactions commonly facilitate CO_2 adsorption, which can be characterized by density functional theory (DFT) and neutron diffraction. DFT for calculating binding energies and charge distributions, while "neutron diffraction" corresponds to the technique used in the literature for locating CO_2 adsorption sites. MOF-74 with various functional groups, such as methyl, amino, fluoro, and lithium alkoxide, has been shown to enhance its selectivity for CO_2 adsorption [57]. DFT was employed to construct models of Ni-MOF-74 and its modified derivative groups. The electrostatic potential gradient on the material surface was quantified by calculating atomic charges (*e.g.*, the Li atom in Li–O–Ni-MOF-74 has a charge of 0.578 eV, and the O atom in the –O–Li group has a charge of –0.42 eV), and the distribution law of the electrostatic potential around organic ligands and metal sites was derived. Combined with the strong quadrupole moment characteristic of CO_2, it was confirmed that the regions with high electrostatic potential gradients could generate specific electrostatic interactions with CO_2, realizing the preferential adsorption of CO_2. Among these materials, the –O–Li modified one exhibited the optimal electrostatic regulation effect [57]. Wu *et al.* [61] have studied the CO_2 adsorption by HKUST-1 and Mg-MOF-74, highlighting the critical role of open metal ions as binding sites as

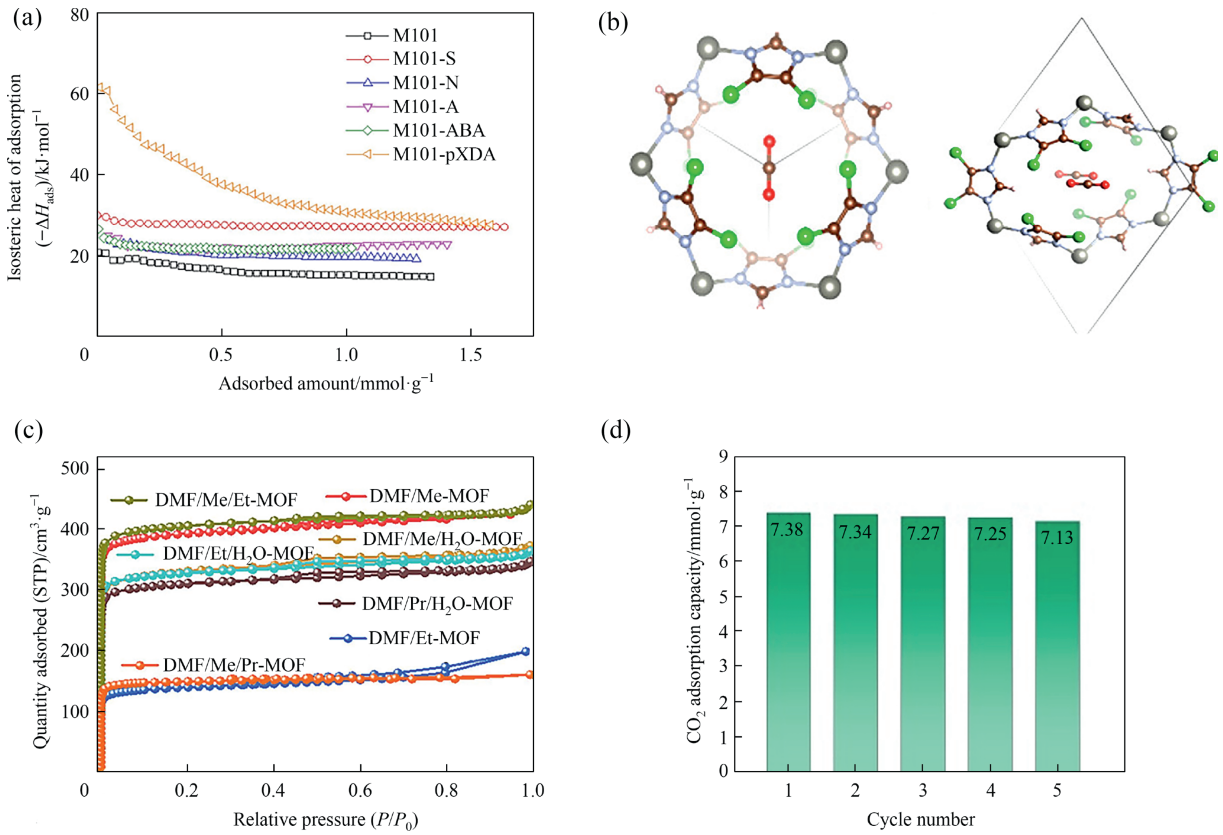


Fig. 8. (a) Isosteric heat calculations for pristine MIL-101-Cr and its functionalized derivatives [39], reprinted with permission from Lee and Jhung, Copyright 2025, Elsevier B.V. (b) The adsorption site of CO_2 within the COK-17 framework [55], reprinted with permission from Wee *et al.*, Copyright 2021, American Chemical Society. (c) N_2 adsorption–desorption isotherms of Mg-MOF-74 tuned by solvent modulation. (d) CO_2 adsorption cycling curves of Mg-MOF-74 [27]. Reprinted with permission from Ma *et al.*, Copyright 2023, Elsevier B.V.

observed by neutron diffraction, verifying electrostatic-dominated physisorption without chemical bonds.

Hydrogen bonding is considered one of the most robust non-covalent interactions, with typical binding energies of less than 40 kJ·mol^{-1}, and is characterized as a form of physical adsorption. This is attributed to its relatively higher binding strength compared to other forms of physical adsorption. Liu *et al.* [62] employed iDPC-STEM to directly visualize the rotational behavior of benzene rings in functionalized UiO-66-X, revealing that functional groups influence CO_2 physisorption by modulating local rigidity, wherein intramolecular hydrogen bonds enhance rigidity, while flexible substituents increase rotational freedom.

Dipole–dipole interactions are manifested between molecules possessing permanent dipole moments. The integration of polar functional groups within MOFs facilitates hydrogen bonding with CO_2, as evidenced by the interactions of oxygen atoms with groups like hydroxyl and amino. Sulfonic acid (SO_3H), noted for its substantial hydrogen bonding potential, acts synergistically with the quadrupole moment of CO_2 to amplify adsorption [43,63]. Researchers [64] have employed DFT calculations to determine various configurations of CO_2 adsorbed onto the zirconium metal centers of UiO-66. Concurrently, static binding energies of CO_2 at distinct sites on the UiO-66 metal centers were analyzed to evaluate the interactions. Computational findings reveal that, on the Zr metal centers, the binding affinity of CO_2 is notably stronger at the hydroxyl (−OH) sites compared to the oxygen (−O) sites and defect locations. This sensitivity of the hydrogen group to gas molecules is attributed to the electrostatic interactions between the negatively polarized oxygen of CO_2 and the positively polarized hydrogen of the hydroxyl group [64]. Amino groups further augment CO_2 adsorption through the formation of hydrogen bonds, thereby facilitating gas capture on the adsorbent surface. The CO_2 capture efficiency of MIL-53(Al) is enhanced by incorporating alcohols such as methanol and isopropanol into its micropores, with an estimated increase of approximately 1.3 times relative to the unaltered framework. Computational analysis has substantiated that hydrogen bonding between the encapsulated alcohols and CO_2 molecules within MIL-53(Al) fortifies the CO_2 capture capability of the framework [65]. The approximate hierarchy of interaction strength, from weakest to strongest, is: van der Waals forces < dipole–dipole interactions < π–quadrupole interactions < hydrogen bonding < electrostatic interactions.

3.2. Chemical adsorption

Chemical adsorption involves chemical interactions between the metal centers or functional groups of MOFs and CO_2, leading to the formation of coordination bonds or chemical complexes [66]. MOFs with open metal sites can establish coordination bonds with CO_2. *In situ* ^{13}C NMR studies have shown that CO_2 exhibits dynamic rotational movements when adsorbed at vacant metal sites [67,68]. Metal centers in MOFs typically possess Lewis acidity, which allows them to interact with the Lewis basic oxygen atoms of CO_2 molecules, forming stable complexes. The electronic configuration, coordination ability, and oxidation state of different metal centers can affect the strength of their interaction with CO_2. Environmental conditions such as temperature and humidity also influence the chemical adsorption of CO_2. Higher temperatures may promote the progress of chemical reactions, while the presence of moisture can compete with CO_2 for adsorption sites.

Meanwhile, the amino groups $-NH_2$ on the ligands of MOFs can interact with CO_2 molecules to form carbamates or carboxylates, thereby affecting chemical adsorption [43]. The amino groups of MOF-808-AA residues interact with CO_2 molecules, resulting in the formation of bicarbonate, carbamate, or carbamic acid. Infrared spectroscopy (IR) has confirmed the changes in the functional groups of the material before and after CO_2 adsorption [69]. Zheng *et al.* [6] used *in situ* IR and DFT calculations to demonstrate that the Zn-OH sites in CFA-Zn-OH can chemically adsorb CO_2 and generate bicarbonate species. DFT calculations indicate that the adsorption of CO_2 is exothermic, with an adsorption energy of -72.1 kJ·mol^{-1}, suggesting that CO_2 desorption can be achieved by heating or purging with an inert gas. Similar to CFA-Zn-OH, MFU-Zn-OH also contains Zn-OH sites, which can achieve efficient CO_2 adsorption by chemically adsorbing CO_2 and generating bicarbonate ions [6]. In addition, Zhu *et al.* [70] synthesized MOF-808-ARG by immobilizing L-arginine on the Zr_6 cluster, achieving water-enhanced CO_2 adsorption and CO_2/C_2H_2 separation performance. *In situ* IR and DFT calculations indicate that in the presence of water, MOF-808-ARG can form bicarbonate products with CO_2. From both thermodynamic and kinetic perspectives, the presence of water is more favorable for CO_2 adsorption than its absence, thereby enabling selective CO_2 adsorption with a CO_2/C_2H_2 selectivity of up to 1180 [70].

As illustrated in Fig. 9, the adsorption mechanisms of CO_2 vary significantly among different functional groups due to their distinct electronic and structural properties. For instance, the sulfonic group ($-SO_3H$) exhibits moderate physical adsorption *via* combined Lewis acid-base interactions and hydrogen bonding: the O atom (Lewis base) interacts with the C atom of CO_2 (Lewis acid), while the H atom (hydrogen bond donor) forms a hydrogen bond with the O atom of CO_2. In contrast, the nitro group ($-NO_2$) relies solely on a weak Lewis acid-base interaction between its O atom and the C atom of the CO_2, resulting in the lowest physical adsorption. The aryl–amino group (aryl–NH_2) exhibits intermediate adsorption performance, involving a Lewis acid-base interaction between the N atom and the C atom of the CO_2, along with hydrogen bonding between the H atom and the O atom of the CO_2. Notably, alkyl–amino groups (*e.g.*, pXDA) enable chemisorption through the formation of stable ammonium carbamate species, requiring two proximate amine groups (~0.75 nm apart) to react

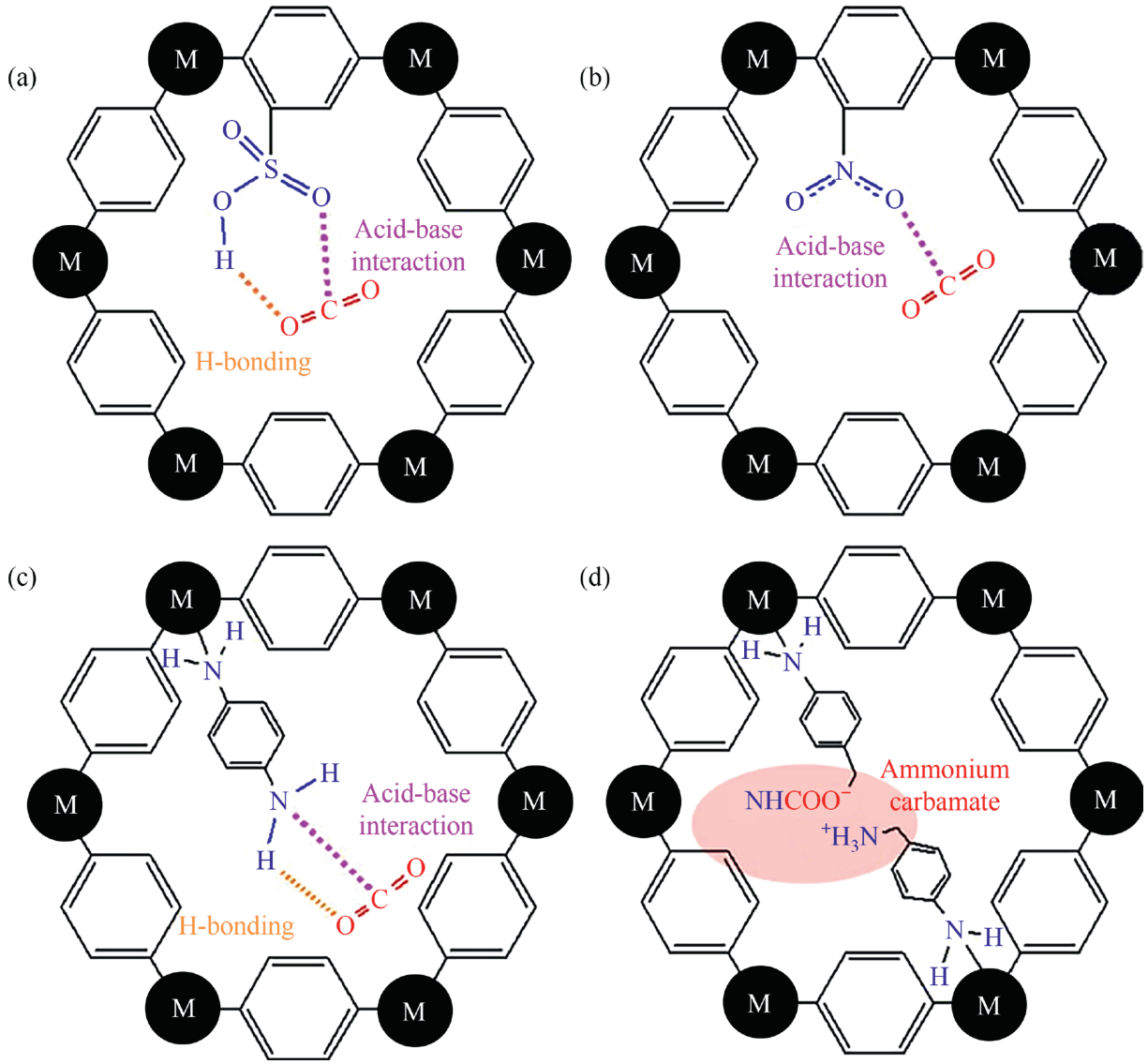


Fig. 9. Proposed CO_2 adsorption mechanisms for (a) $-SO_3H$, (b) $-NO_2$, (c) aryl–NH_2, and (d) alkyl–NH_2 functional groups [39]. Reprinted with permission from Lee and Jhung, Copyright 2025, Elsevier B.V.

sequentially with CO_2, yielding high adsorption heat, large capacity, and excellent selectivity [39].

It is challenging to completely differentiate between physical and chemical adsorptions, as they often co-occur. Nonetheless, within a given system, one form of adsorption may be predominant. In essence, physical adsorption involves intermolecular forces, with adsorption enthalpies ranging from 0 to 40 $kJ \cdot mol^{-1}$, and is reversible, allowing desorption to occur through an increase in temperature. Chemisorption consists of the formation of new chemical bonds, such as covalent or ionic bonds. This process is characterized by high adsorption enthalpies, typically >80 $kJ \cdot mol^{-1}$, and is generally irreversible or difficult to reverse, requiring elevated temperatures for desorption.

4. Theoretical Calculations of CO_2 Capture by MOFs

4.1. DFT calculation

When studying the adsorption of CO_2 in MOFs, DFT calculation is one of the quantum mechanical methods used to analyze the interaction between CO_2 and MOFs, determine the adsorption sites, calculate the adsorption energy, charge distribution, and changes in the geometric structure of CO_2. Previously, Tassé *et al.* [71] employed DFT, combined with the Bader charge analysis method, to investigate charge transfer during the CO_2 adsorption process. The amount of charge obtained by CO_2 varies at different sites of MOF-808, and the charge transfer amount is relatively small, indicating that the interaction between CO_2 and MOFs is mainly physical adsorption. In addition, Tassé *et al.* [71] used DFT to calculate the changes in the geometric structure of CO_2 during the adsorption process, including the O—C—O bond angle and the shortest distance between CO_2 and the MOF. They found that the values vary at different sites, suggesting that CO_2 may undergo slight deformation during adsorption, but the overall structural change is not significant.

4.2. Molecular simulation

Molecular simulations, including grand canonical Monte Carlo (GCMC) and molecular dynamics (MD), are powerful tools for analyzing CO_2 adsorption and diffusion in MOFs. GCMC simulation, based on statistical mechanics, can analyze the mechanism of gas adsorption and separation and predict adsorption isotherms. Researchers [72] have constructed functionalized MOFs (Zr-NDC-X, NDC = naphthalene-2,6-dicarboxylic acid, X = $-NO_3$, $-NH_2$ and $-SO_3H$) with different polar groups. GCMC simulations indicate that at low pressure, polar groups can enhance CO_2 adsorption, with stronger polarity resulting in a more pronounced increase. However, at high pressure, the CO_2 adsorption advantage of functionalized MOFs disappears due to enthalpic and entropic effects. Also, the N_2 adsorption capacity of Zr-NDC-X is higher than that of Zr-NDC across the entire pressure range. At low pressure, the enthalpic effect is significant, and at 3 MPa, the entropic effect becomes pronounced. Studies on Zr-NDC-SO_3H indicate that the MOF solid surface allows direct interaction between functional groups and CO_2 through strong hydrogen bonds, while N_2 shows no significant interaction with the functional groups. Functionalized MOFs have higher CO_2 selectivity than Zr-NDC. As the polarity of the functional groups increases, both the working capacity and CO_2 adsorption affinity rise [72].

Oktavian *et al.* [73] used RASPA molecular simulation software for GCMC simulations and found that CO_2 adsorption capacity is influenced by adsorption heat and pore size. Cai *et al.* [74] employed MD simulations to investigate the adsorption performance of IRMOF-1 to IRMOF-5 for CO_2, revealing that functional groups on organic ligands affect adsorption capacity and selectivity. Among them, IRMOF-4 showed high CO_2 adsorption and selectivity due to the strong interaction between its $-OC_3H_7$ group and CO_2 molecules. MD simulations also demonstrated that CO_2 diffuses more slowly than N_2 in MOFs, which benefits CO_2/N_2 separation.

Song *et al.* [75] used MD simulations to study the mass transfer resistance between MOFs and CO_2. MD simulations assess gas transport properties in MOFs by integrating Newton's equations of motion, such as self-diffusion coefficients. Results showed that CO_2 experiences stronger transport resistance than CH_4 under the same conditions due to higher energy barriers, larger molecular weight, stronger interactions, and partial loss of degrees of freedom [75]. MD simulations are beneficial to understand the dynamic behavior of gas molecules in MOF pores. Functionalized MOFs with polar groups show enhanced CO_2 adsorption and selectivity, particularly at low pressures, and MD simulations further reveal how functional groups and linker properties influence CO_2 and N_2 diffusion. Overall, these simulation methods provide crucial theoretical guidance for designing MOFs with efficient CO_2 capture capabilities.

4.3. Artificial intelligence

Artificial intelligence (AI) integrates high-throughput computing, machine learning, and molecular simulations to form a smart platform for material discovery and optimization. Machine learning, a subset of AI, enables computers to learn from data and predict the performance of new MOFs, guiding synthesis and optimizing preparation processes. It can swiftly predict CO_2 adsorption capacity and selectivity of MOFs, accelerating material discovery. For instance, machine learning identified NOTT-101/OEt as a high-performing MOF for CO_2 capture, with experimental results matching predictions [76]. However, AI's effectiveness in MOFs for CO_2 adsorption has limitations. The performance of machine learning models hinges on the quality and quantity of training data. Noisy, biased, or insufficient data can compromise the accuracy of predictions. Additionally, training complex models demands significant computational resources, posing a challenge for some teams. Furthermore, AI predictions must be experimentally validated, as practical uncertainties can cause discrepancies with model predictions [76].

Moreover, high-throughput computational screening (HTCS), leveraging molecular simulations, can rapidly screen numerous MOF materials. Researchers use HTCS to evaluate thousands of MOF candidates for CO_2 capture. In CO_2 capture studies, MOFs from various databases are assessed for their CO_2 adsorption capability. For example, Li *et al.* [77] conducted GCMC simulations on 15333 computationally ready, experimentally synthesizable MOF database (CoRE-MOFs) under specific conditions to compute the adsorption properties of CH_4/CO_2 mixtures. This generated extensive adsorption data for diverse MOF structures, aiding in the identification of promising materials for CO_2 capture.

5. Strategies for Enhancing CO_2 Adsorption in MOFs

5.1. Optimization of pore size and shape

MOFs have a significant advantage over conventional materials in controlling the size of pores and structural design, allowing pores to be precisely adjusted through simple synthesis and modification processes. The size of the pores directly affects the diffusion path of gas molecules and the likelihood of contact with adsorption sites. In contrast, the uniform distribution of pores increases the diffusion resistance, allowing gas molecules to diffuse into the material. The size of pores is a crucial factor in determining whether a CO_2

molecule enters the structure of the pores or the adsorption sites of metal centers and organic ligands, such as polar functional groups. A larger pore distribution provides more space for CO_2 storage, thereby increasing the adsorption capacity. The following are the key ways to control MOF pore size. Adjusting the selection and ratio of solvents, the choice and proportion of solvents have a significant impact on the growth and pore size of MOF crystals. For instance, increasing the ratio of water to ethanol can lead to larger crystal sizes. Campbell and Tokay [78] introduced a new method for modulating the crystal dimensions and morphology of Mg-MOF-74 by utilizing the solvent composition as a controlling factor. It was found that the solvent composition plays a crucial role in influencing both the nucleation rate and the final crystal size. Moreover, specific structural guide agents can change the pore structure of MOFs. Adding PVP during UiO-66-$(OH)_2$ synthesis improved selective CO_2 adsorption over N_2 by promoting uniform dispersion of MOF particles [79].

By finely tuning the synthesis and post-synthesis modification processes of MOFs, it is possible to adjust the pore characteristics, thereby affecting the pore size [80,81]. For instance, Shi *et al.* [82] reported the synthesis of MOF-74-Co with tunable particle size and superior quality, characterized by its uniform particles, high crystallinity, and substantial specific surface area. The smaller MOF-74-Co variant (78 nm) exhibited superior CO_2 adsorption kinetics and higher saturation capacity compared to larger samples. Banerjee *et al.* [19] synthesized and characterized eight ZIFs, including ZIF-78, which demonstrated the highest CO_2 adsorption capacity among them. Bastin *et al.* [83] synthesized MOF-508b and evaluated its effectiveness in separating CO_2 from various gas mixtures, highlighting its high selectivity for CO_2 at a specific pore size of 0.4 nm × 0.4 nm. An and Rosi [84] modified the CO_2 adsorption capacity of MOF-1 through cation exchange, altering pore volume and surface area. Notably, the β-cage aperture of ZIF-8, measuring approximately 0.34 nm, is slightly smaller than the kinetic diameter of a CO_2 molecule (0.33 nm), which plays a crucial role in size-selective separation at the molecular level [85].

5.2. Surface functionalization strategy

By incorporating ligands with diverse functional groups into the MOF structure, the adsorption of CO_2 can be significantly enhanced. Ligand functionalization modification involves attaching the target functional groups to the ligands before the synthesis of MOFs, ensuring that these groups remain attached to the ligands after synthesis, thereby achieving the purpose of introducing the target functional groups. This strategy has been explored by Cmarik *et al.* [86], who synthesized UiO-66 variants modified with various ligands to assess their impact on polarity, basicity, and hydrophobicity, ultimately revealing that amino-functionalized UiO-66 displayed superior CO_2 adsorption attributes. Amino functional groups (such as $-NH_2$, alkyl amines, *etc.*), amide functional groups, other nitrogen-containing functional groups (such as azide, triazole, pyridine, *etc.*), polar functional groups (such as $-OH$, $-COOH$, $-NO_2$, $-SO_3H$, *etc.*), and phenyl functional groups ($-C_6H_5$) can all enhance the adsorption of CO_2. The high polarity characteristic enhances adsorption through dipole–dipole interactions, hydrogen bonds, *etc.*, interacting with CO_2 (a molecule with a strong quadrupole moment) [87].

Fig. 10 presents four modified MIL-53 structures: $(CH_3)_2$-MIL-53, $(OH)_2$-MIL-53, NH_2-MIL-53, and COOH-MIL-53, labels the CO_2 adsorption sites in each structure (such as Site A, Site B, *etc.*), and provides the binding energy (BE, kJ·mol^{-1}) and intermolecular distance (nm) for each site. The more negative the binding energy, the stronger the interaction between CO_2 and the adsorption site. The binding energy of Site A in COOH-MIL-53 is −21.5 kJ·mol^{-1},

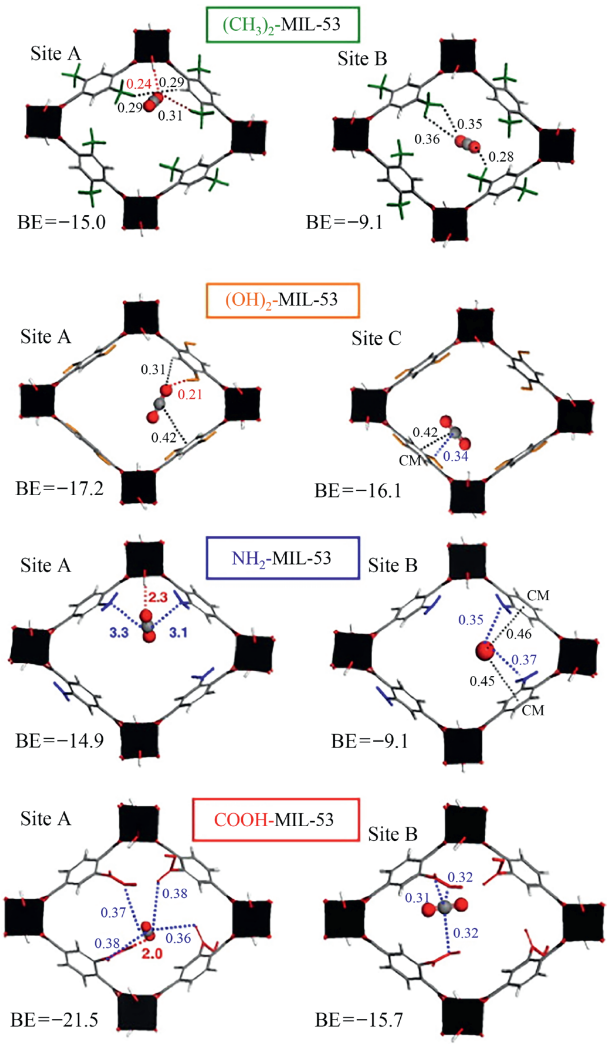


Fig. 10. In MIL-53(Al) structures modified with different functional groups ($(CH_3)_2$, $(OH)_2$, NH_2, and COOH), the main adsorption sites of CO_2 and related parameters [87]. Reprinted with permission from Soleimani *et al.*, Copyright 2024, Elsevier BV.

which is significantly higher than the corresponding sites in structures modified with other functional groups, indicating that the interaction between the COOH functional group and CO_2 is stronger, which is also an important reason for its ability to enhance CO_2 adsorption performance. Fig. 10 intuitively demonstrates the mechanism by which polar functional groups improve adsorption capacity by changing the chemical environment of adsorption sites and enhancing interactions with CO_2 molecules (which have a strong quadrupole moment) [87].

5.3. Metal site regulation strategy

It is well-known that the open metal site in MOFs is a key adsorption site for CO_2 [51,85]. By leveraging the quadrupole moment of CO_2, these open metal sites facilitate electrostatic interactions that enhance CO_2 adsorption [88]. For instance, Norouzbahari *et al.* [88] utilized open metal sites in Zn-MOF-74 to develop a core–shell structure of ZIF-8@Zn-MOF-74, which achieves the synergistic effect of ZIF-8 (providing molecular sieving functionality) and Zn-MOF-74 (endowed with open metal sites and large pore size). The CO_2 adsorption capacity of the core–shell structured MOF reaches 3.27 mmol·g^{-1}, which is 63.5% higher

than that of pristine ZIF-8. The reason for this enhancement lies in the electrostatic interactions between the open metal sites in the Zn-MOF-74 shell and CO_2. Abid *et al.* [89] enhanced both the CO_2 adsorption capacity and selectivity for CO_2/N_2 in MIL-53(Al) by doping with Mn^{2+} enhancing the open metal sites and basic sites of manganese oxide. The introduction of Mn^{2+} synergistically enhances the adsorption performance through electrostatic interactions between basic sites and CO_2 and the microporous sieving effect. Although this enhancement significantly improves the adsorption performance, introducing Mn^{2+} may compromise the integrity of the material's crystal structure. Prolonged exposure to humid air poses risks such as hydrate formation or hydrolysis reactions that could affect the cyclic service life of the material. Therefore, it is essential to conduct comprehensive research on optimizing doping concentrations or implementing post-treatment strategies to balance between enhanced adsorption performance and stability.

For MOFs containing multiple metal sites, it is crucial to investigate their synergistic adsorption mechanisms and potential interference factors. The effective combination of alkali metal cations and NH_2-MIL-101 was achieved *via* a post-modification method. The CO_2 adsorption capacity of 0.1K-NH_2-MIL-101 reached 8.2 $mmol \cdot g^{-1}$, which was 3.2 times that of pristine NH_2-MIL-101 (2.9 $mmol \cdot g^{-1}$). Mechanistically, alkali metal cations, especially K^+, induced electron density redistribution around oxygen atoms in the MOF framework through electrostatic interactions with carboxylate (COO^-) groups, thereby significantly enhancing the adsorption affinity towards CO_2 molecules [90]. By employing advanced characterization techniques and simulations, the synergistic adsorption pathways, rate-limiting steps, and interference factors of multiple metal sites can be dissected. Subsequently, the metal ratios and synthesis conditions can be optimized to achieve the synergistic enhancement of multiple metal sites. This approach offers new perspectives for designing MOFs with highly efficient adsorption capabilities for CO_2 capture.

5.4. Crystal facets regulation

The connection between crystal facet arrangement and CO_2 adsorption performance is well demonstrated in Ni-MOF systems. Through controlled synthesis conditions, Ni-MOF(H_2O) predominantly exposes the (010) facet with 29.2% surface O—H groups, significantly higher than the 14.7% in Ni-MOF, where the densely packed (200) facet dominates. This facet difference leads to markedly stronger CO_2 adsorption on Ni-MOF(H_2O), with DFT calculations confirming an adsorption energy of −0.85 eV *vs.* −0.62 eV for Ni-MOF, and a shorter Ni—C bond length (0.187 nm *vs*. 0.195 nm) [91].

Similarly, in G-MOF-74 systems, facet variation through morphology control directly impacts adsorption capacity. The slender nanorod G1-MOF-74 exhibits 39.5% higher CO_2 uptake (5.86 $mmol \cdot g^{-1}$) than the stubby nanorod G2-MOF-74 (4.2 $mmol \cdot g^{-1}$), attributable to its optimized facet configuration that provides better access to active sites, coupled with its larger surface area (1183.4 $m^2 \cdot g^{-1}$ *vs*. 733.6 $m^2 \cdot g^{-1}$) [92]. These examples quantitatively demonstrate how targeted facet exposure enhances CO_2 adsorption through optimized surface chemistry and improved active site accessibility.

5.5. Defect engineering strategy

It is generally known that the introduction of defects into MOF crystals (through chemical etching or controlled synthesis conditions) serves as adsorption centers for CO_2, enhancing the adsorption capacity. MOFs possess certain defect types that are particularly significant in enhancing CO_2 adsorption. During the MOF synthesis process, ligand defects are formed when their ligands are replaced by ions such as chlorides, hydrogen, monocarboxylic acids, or solvent molecules. This substitution event leads to the disruption of the regular periodic lattice structure of MOFs, which in turn causes an enlargement in pore size and an increase in porosity. Consequently, the performance of MOFs in CO_2 adsorption is modified [93]. Understanding the precise impact of different substituting species on the defect formation and subsequent CO_2 adsorption characteristics could be an area worthy of further exploration. Therefore, it is essential to understand the effect of the electronic properties of the substituting ions or molecules interacting with the MOF framework on the adsorption behavior. Moreover, investigating the stability of these defect-induced structures over extended periods and under varying environmental conditions would provide valuable insights for practical applications [94]. Zhang *et al.* [95] adopted a crystal defect method, utilizing organic acids to prepare hierarchically porous Mg-MOF-74. Incomplete or missing metal nodes, which can be considered a form of defect, have the potential to create active sites that significantly impact the adsorption of gas molecules [96].

Defective UiO-66(Zr)-$(OH)_2$, regulated by acetic acid, shows a significant enhancement in CO_2 adsorption capacity [41]. This relationship between defect concentration and adsorption capacity prompts questions about the optimal defect levels for maximizing CO_2 adsorption while maintaining the stability of the MOFs. Further investigations could involve exploring different modulators or reaction conditions to precisely control the defect concentration and understand how it correlates with other properties such as selectivity and long-term stability. Feng *et al.* [9] synthesized bimetallic (Zn, Zr)-UiO-66 by altering the ratio of zinc to zirconium. Through a soft acid treatment, the less stable zinc nodes were selectively removed, resulting in UiO-66 with cluster defects. The findings indicated that these cluster defects promote both CO_2 adsorption and CO_2/N_2 selective adsorption [9]. This approach of creating specific defects through selective node removal offers a novel way to engineer MOFs for improved gas separation applications.

During MOF-74 synthesis, DMF releases the formic acid that coordinates with magnesium and occupies the open metal sites of Mg in MOF, thereby reducing CO_2 adsorption performance [97]. However, research has discovered that the incorporation of acetic acid can lead to the presence of missing linker defects within MOF materials, thereby improving CO_2 adsorption performance [64]. These two perspectives may seem contradictory, but in essence, both underscore the importance of defects in MOFs. Solvent-derived formate defects are formed by formic acid derived from the decomposition of solvents, such as DMF, during the synthesis of MOFs. They may be randomly distributed throughout the MOF structure, competitively binding to open metal sites. During the synthesis of MOFs, the addition of acetic acid can control crystal growth and promote the formation of defects. These defects may be orderly and could serve different functions within the structure, such as increasing porosity or altering pore size. Missing linker defects may lead to uneven local charge distribution within the material. Consequently, stress concentration can occur during high-pressure CO_2 adsorption, affecting the structural stability of the material. In contrast, the framework vacancies caused by missing-cluster defects may reduce the tolerance of the material to small-molecule impurities, making it prone to irreversible adsorption and pore blockage. Therefore, future research should focus on developing novel defect control techniques to precisely regulate the location, quantity, and type of defects, to mitigate these negative effects, and maximize the enhancement of adsorption performance.

6. MOF Composite Materials

To further enhance the CO_2 adsorption efficiency of MOFs or endow them with additional functionalities, hybridization with other materials has been recognized as a viable strategy. The significance of compositing MOFs with other materials is rooted in overcoming the performance limitations of single-component systems and the integration of multifunctionalities through synergistic effects. When combined with porous carbons, polymers, or other substrates, the high specific surface area and abundant adsorption sites of MOFs can be complemented by the mechanical robustness and chemical stability of the supporting materials, leading to a notable improvement in CO_2 adsorption capacity and cycling stability. The incorporation of functional moieties such as amino groups or ionic liquids can enable chemisorption capabilities or humidity-responsive properties to be introduced to MOFs, addressing the challenges of structural instability and insufficient selectivity in humid environments. Additionally, the design of composite structures such as core–shell or hierarchical porous architectures allows for precise regulation of pore size distribution and diffusion pathways, with mass transfer kinetics and adsorption selectivity being optimized as a result. These aspects will be discussed in detail in the subsequent sections.

6.1. Carbon–MOF composites

MOFs are admired for their exceptional porosity, however, their affinity for small gas molecules is often insufficient, resulting in the underutilization of their expansive voids for gas storage. To address this, the integration of MOFs with other porous materials is a strategic approach to creating composite materials that can surpass the limitations of individual components [98]. MOF/graphene oxide (MOF/GO) composites are synthesized *in situ* by blending MOF precursors with GO under controlled conditions, such as temperature and pressure, to create a material that leverages the porosity and active sites of MOFs and the dense carbon atom arrangement of GO [99]. This combination not only enhances dispersive interactions but also potentially improves the chemical and thermal stability of the composite [100]. The composite mechanism of MOF/GO is multifaceted, involving surface active sites where oxygen-containing functional groups on GO can interact with MOF components, providing additional adsorption sites and potentially creating new pore structures at the interface [98]. The carbon atom array of GO also contributes to the dispersion of MOF crystals, enhancing the overall performance of the material, while charge transfer between MOFs and GO can influence the electronic properties and adsorption capacity of the composite.

The integration of MOFs and GO can be achieved through physical or chemical means, with chemical bonding often involving covalent or hydrogen bonds. The MOF crystals can grow *in situ* on GO, promoting the stability of the composite. The MOF-505@GO composite has demonstrated the highest CO_2 adsorption capacity of 3.94 $mmol \cdot g^{-1}$ at 298 K and 100 kPa, which is a 37.3% increase compared to the original MOF-505 [101]. The MOF-505@GO exhibits CO_2/CH_4 and CO_2/N_2 adsorption selectivities of up to 37.2 and 8.6, respectively, significantly higher than the original MOF-505. The reason is that the introduction of GO can increase the surface dispersive forces of the composite material, as GO has a dense array of atoms and rich oxygen functional groups, which can enhance the adsorption of CO_2 molecules. The introduction of GO may also generate more unsaturated metal sites within the MOF-505 units. These sites can act as strong adsorption sites, enhancing the adsorption capacity for CO_2. This synergistic effect may stem from the interactions between GO and MOF-505, which not only increase the pore volume but also enhance the affinity for adsorbed molecules [101].

By combining GO with MOFs, the chemistry and microstructure of the MOF units are altered, resulting in synergistic features that are beneficial for CO_2 capture. Cu-BTC/aminated GO composites serve as highly efficient CO_2 capture media. This composite material shows a significant improvement in CO_2 adsorption performance compared to the original Cu-BTC MOF. In particular, the MOF/GO-U3 composite demonstrates excellent CO_2 adsorption capacity and a fully reversible adsorption process, capable of restoring its CO_2 adsorption capacity without the need for thermal treatment, indicating its structural stability under operating conditions [102]. The synthesized UiO-66/GO composite showed a remarkable CO_2 adsorption rate of 3.37 $mmol \cdot g^{-1}$, a 64.8% increase from pure UiO-66, compared to conventional active carbon and zeolites [103].

While carbon nanotubes are beneficial for CO_2 capture, the chemical property disparity between nanotubes and MOFs can lead to weak interfacial binding and potential delamination during cyclic adsorption. This observation underscores the need for innovative surface modification techniques or chemical bonding strategies to enhance the synergy and stability of these composite materials. The development of such strategies is crucial for gas storage and capture applications, highlighting a significant area for future research and development.

6.2. Chitosan–MOF composites

Chitosan serves as a template, with its molecular −OH and $-NH_2$ groups capable of coordinating with the metal centers of MOFs to form active sites, which further interact with organic ligands to form chitosan–MOF composite materials. This *in situ* growth method allows MOFs to grow directly on the chitosan template, which is beneficial for controlling the distribution and morphology of MOFs within the chitosan matrix [104,105]. Chitosan acts as a structural directing agent during the growth of HKUST-1 crystals. In the HKUST-1@Chitosan composite material, smaller HKUST-1 particles are formed inside the chitosan microspheres, while larger particles are formed on the surface. This is because the nitrogen-containing functional groups inside the chitosan microspheres have a limiting effect (*i.e.*, steric hindrance effect) on the growth of HKUST-1 particles, resulting in smaller internal particles.

Furthermore, there are relatively more metal ions and greater spatial freedom nearer to the surface, which is conducive to the expansion of the HKUST-1 network and crystal growth, thus forming larger particles. Chitosan provides a stable framework for HKUST-1 crystals, preventing their structural collapse under adsorption conditions. This is because chitosan has a certain mechanical strength and stability, and can maintain the structural integrity of HKUST-1 during the gas adsorption and desorption processes, thus ensuring the stability and repeatability of the adsorption performance of the composite material. The presence of chitosan also helps to improve the mechanical stability of the composite material. The average compressive strength of HKUST-1@Chitosan aerogel reaches 12.35 N, making it suitable for practical application scenarios [105]. Fig. 11 illustrates the *in situ* development of HKUST on chitosan to form chitosan–MOF composite materials [105].

6.3. DES–MOF composites

Deep eutectic solvents (DES) are a new class of analog ionic liquids that are considered to be environmentally friendly [106]. They are formed by the combination of hydrogen bond receptors

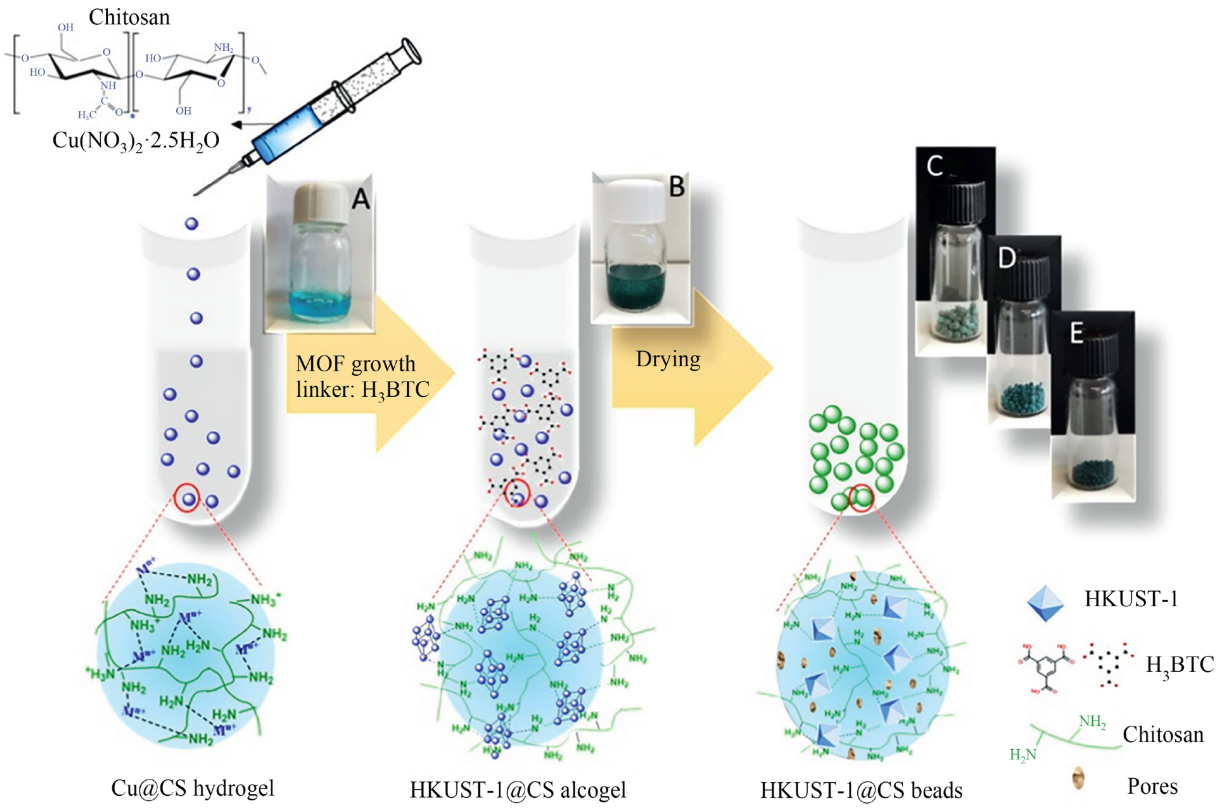


Fig. 11. Flow chart of *in situ* growth of HKUST on chitosan to form composite materials [105]. Reprinted with permission from Hammi *et al.*, Copyright 2023, American Chemical Society.

(HBAs) and hydrogen bond donors (HBDs) through hydrogen bond interactions without further cleaning; they can be used directly after synthesis, with a 100% utilization rate of atoms, so that they are truly green solvents. DES is less toxic than traditional organic solvents and less harmful to analysts and researchers. DES can be adapted to different applications, changing structures and ratios, extracting, separating, and analyzing target compounds. MOFs modified by DES improve adsorption performance [107]. The utilization of DES to modify MOFs can enhance CO_2 adsorption through multiple mechanisms. Firstly, DES can introduce supplementary functional groups onto the MOF surface. Secondly, DES modification might induce alterations in the MOF structure that enhance its porosity, providing more space for CO_2 adsorption. Thirdly, DES can be utilized to adjust the pore size of MOFs. Moreover, this modification can enhance the thermal and chemical stability of MOFs. Additionally, the components of DES can engage in chemical interactions with CO_2. For instance, when amine groups are present in the DES, carbamates can be formed, leading to a higher CO_2 uptake [108].

Amino-rich DES are dispersed on the surface of MOF-808, achieving efficient CO_2 capture. This composite material maintains its microporous structure while demonstrating excellent CO_2 adsorption capacity, kinetics, CO_2/N_2 selectivity, and isosteric heat of adsorption. The optimized sample DES-2@MOF-808-FR exhibits a significant CO_2 adsorption capacity of 4.16 $mmol \cdot g^{-1}$ at 298 K and 0.1 MPa, and maintains a working capacity of 2.86 $mmol \cdot g^{-1}$ and a CO_2/N_2 selectivity of 1184 in simulated flue gas, surpassing most existing materials [5]. Zhang *et al.* [109] modified ZIF-8 using a DES, resulting in a "core–shell" structure. The CO_2/N_2 separation selectivity of ZIF-8 was 72.77, and following DES modification, it could reach 997.50, representing a 13.71-fold increase compared to the original ZIF-8. The DES-modified UiO-66-COOH complex, which is formed by combining the amine and hydroxyl groups of DES with the open metal site of UiO-66, helps to improve the CO_2 capture, and the CO_2 adsorption capacity is 26% higher than that of the original UiO-66 [49].

The metal–organic skeleton NH_2-MIL101(Cr) was modified by a deep eutectic solvent composed of choline chloride and urea, and the adsorption capacity was increased by 1.7 times [110]. This enhancement is due to the synergistic interaction between adsorbents and DES, which is confined in the pores. DES-modified NH_2-MIL101(Cr) has a strong binding affinity with CO_2 molecules [110]. These findings highlight the potential of using DESs to modify MOFs for improved CO_2 adsorption. Future research could focus on exploring more combinations of DES components and MOF structures to further fine-tune the adsorption characteristics and understand the underlying mechanisms in greater detail.

6.4. Polymer–MOF composites

A composite material that incorporates a conductive polymer into MOF can improve the electrochemical performance and gas adsorption selectivity of MOF, and improve the adsorption kinetics and selectivity. These polymers likely improve the conductivity of the MOFs and offer extra sites for gas molecule interaction, which can result in enhanced adsorption kinetics and selectivity for specific gas separation tasks. The MOF-74PH (polyHIPE) composite material uses a combination of Pickering HIPE (high internal phase emulsion) polymerization and MOF secondary refractive. Compared to the MOF-74 powder, composite materials show higher adsorption capacity, faster adsorption kinetics, and better CO_2 adsorption performance and regeneration efficiency. The resulting MOF-74 polyHIPE composite monoliths have high porosity and co-continuity, presenting a large macro-

microporosity architectural hierarchy, favoring gas capture applications [111].

SIFSIX-3-Ni/PAN (SIFSIX-3-Ni stands for the abbreviation of Silicon-Fluoride, where "Ni" indicates that Nickel is the metal center. PAN is the abbreviation for polyacrylonitrile.) composite beads possess significant application potential in CO_2 capture, especially in situations requiring the handling of low CO_2 concentrations. The composite material exhibits a hierarchical porous structure, including macropores, mesopores, and micropores, which facilitates rapid adsorption processes. This approach effectively regulated the MOF content, enabling the synthesis of composite materials with up to 70% MOF loading [112]. A reliable synthetic method was utilized to produce millimeter-scale composite beads of MOF and PVDF with varying PVDF binder proportions. The fabrication process involved a phase inversion technique followed by post-synthetic modification with 1-ethylpropane-1,3-diamine. The 1-ethylpropane-1,3-diamine-grafted-MOF/PVDF40 demonstrated enhanced durability and structural integrity over up to one month, surpassing the original MOF powder [113]. The composite material not only has high porosity and a hierarchical pore structure but also exhibits excellent mechanical stability and regeneration efficiency, providing an innovative solution for efficient and sustainable CO_2 capture.

Besides, the integration of MOFs with polymers to form membrane materials combines the exceptional gas adsorption capabilities of MOFs while addressing the limitations of pure MOF membranes in terms of mechanical strength, processability, and stability, thereby facilitating more efficient CO_2 capture. The mixed-matrix membranes (MMMs), which combine inorganic fillers within a polymer matrix, amalgamate the high-performance attributes of inorganic membranes with the facile fabrication of polymeric membranes [114]. The synthesis of MOF-incorporated membrane materials can be achieved by *in situ* growth, sol–gel process, self-assembly technique, or the physical blending of MOFs into polymer membranes. Li *et al.* [115] fabricated MMMs by integrating ultra-small ZIF-7 nanoparticles, with a size range of approximately 30–35 nm, into a Pebax®1657 polymer matrix. These composite membranes exhibit robust interfacial adhesion. The incorporation of ZIF-7 nanoparticles augments the selectivity and permeability for CO_2/N_2, presumably due to the combined effect of the molecular sieving capabilities and the high CO_2 solubility of ZIF-7 in Pebax®1657 [115].

By physically mixing and solvent evaporation techniques, MIL-53(Al) and MWCNT (multi-wall carbon nanotubes) are uniformly dispersed in the PES (polyethersulfone) polymer matrix, forming the PES/MIL-53(Al)@MWCNT mixed matrix membrane [116,117]. The addition of MWCNT helps to improve the dispersion of MIL-53(Al) in the polymer matrix, enhancing the mechanical properties. Besides, the interaction between MWCNT and MIL-53(Al) provides a fast transport channel for CO_2 molecules, thereby improving the CO_2 permeability and selectivity on the membrane [116,117]. The MOF-801/PEBA (polyether block amide) mixed solution is deposited onto a porous material. The MOF-801 nanoparticles and the PEBA polymer form a synergistic mixed-matrix structure to exhibit outstanding performance in CO_2 capture [118]. By growing NENP (nitrogen-enriched nanoporous polytriazine) on the surface of ZIF-8 and functionalizing it with ethylenediamine, a core–shell structure is formed, which helps to improve the transport and separation efficiency of CO_2 [119]. The chemical environment of the NENP pores is adjusted by the impregnation of ethylenediamine, enhancing the compatibility with the polymer matrix and thereby improving the overall performance of the material. These advantages make ZIF-8@NENP-NH_2 a potential high-performance material for CO_2 capture and separation.

6.5. Ionic liquid–MOF composites

Ionic liquids can serve as additives for MOFs to enhance the adsorption of CO_2 [120]. Ionic liquids (ILs) capable of capturing CO_2 come in a variety of types, and due to their unique physicochemical properties [10]. Fig. 12 describes predominant IL cations and anions. They are considered promising alternatives to traditional amine solvents [121].

Imidazolium-based ILs typically have good chemical and thermal stability, such as 1-alkyl-3-methylimidazolium cations. Pyridinium-based ILs have good air and moisture stability, with common cations like tetrabutylpyridinium cations [121]. Quaternary ammonium-based ILs have good biocompatibility, with common cations like tetramethylammonium cations. Phosphate-based ILs have better conductivity and are suitable for electrochemical applications. Sulfate and sulfonate-based ILs typically have good water solubility and are suitable for aqueous reactions and separation processes. Fluoride-based anionic ILs have excellent electrochemical stability and are ideal for high-energy batteries and electrochemical sensors. Task-specific ILs are designed for specific applications, such as ILs for CO_2 capture, which may contain specific functional groups to enhance the adsorption capacity for CO_2. Surface-active ILs contain long-chain alkyl groups and exhibit properties similar to traditional surfactants, capable of forming self-assembled structures like micelles, vesicles, and liquid crystals. Supported ILs are immobilized on a solid support to improve their stability and reusability in certain applications. Amino acid-functionalized ILs ([BMIm]Gly and [BMIm]Arg) were loaded onto amino group-containing MOFs, NH_2-UiO-66(Zr) and NH_2-MIL-125(Ti), to prepare new IL composite materials that can enhance CO_2 adsorption capacity and selectivity. In the 50% (mass) [BMIm]Arg-NH_2-UiO-66(Zr) composite material, new ultra-micropores (<0.65 nm) were formed, which play an important role in improving the adsorption capacity and selectivity of CO_2. By constructing synergistic adsorption effects in IL composites and forming micropores and ultra-micropores, trace CO_2 can be effectively removed from air and confined spaces [122].

6.6. Zeolite–MOF composites

The integration of zeolite and MOFs presents an effective strategy to capitalize on the regular pore channels and excellent thermal stability of zeolites, thereby enhancing the adsorption and separation efficiency of CO_2. Core–shell zeolite 5A@MOF-74 composites, for instance, amalgamate the properties of zeolite and MOF-74 for CO_2 adsorption purposes [123]. The new composite material 0.5HZSM-5@Mg-MOF-74 is a zeolite@MOF composite material that can simultaneously capture CO_2 and H_2O from the air. Compared with Mg-MOF-74, the composite material exhibits higher water adsorption capacity and structural stability. The metal nodes of Mg-MOF-74 interact with the surface functional groups of the zeolite, increasing the number of metal active sites and porosity. Synthesizing the composite material enhances the CO_2/H_2O co-adsorption performance of Mg-MOF-74 [124].

The zeolite-5A@MOF-74 composite exhibited a 20% to 30% enhancement in CO_2 uptake relative to the unmodified MOF. The reason is that the composite material has increased surface area and pore volume compared to the single material [123]. Additionally, the ZSM-5@MOF-199 composite adsorbent was synthesized at room temperature. Modifying the zeolite core to protonic hierarchical ZSM-5 achieved a 28% increase in CO_2 uptake [125]. The ZSM-5@MOF-199 core–shell composite adsorbent combines the acidity and high hydrothermal stability of ZSM-5 with the large pore diameter and metal active sites of

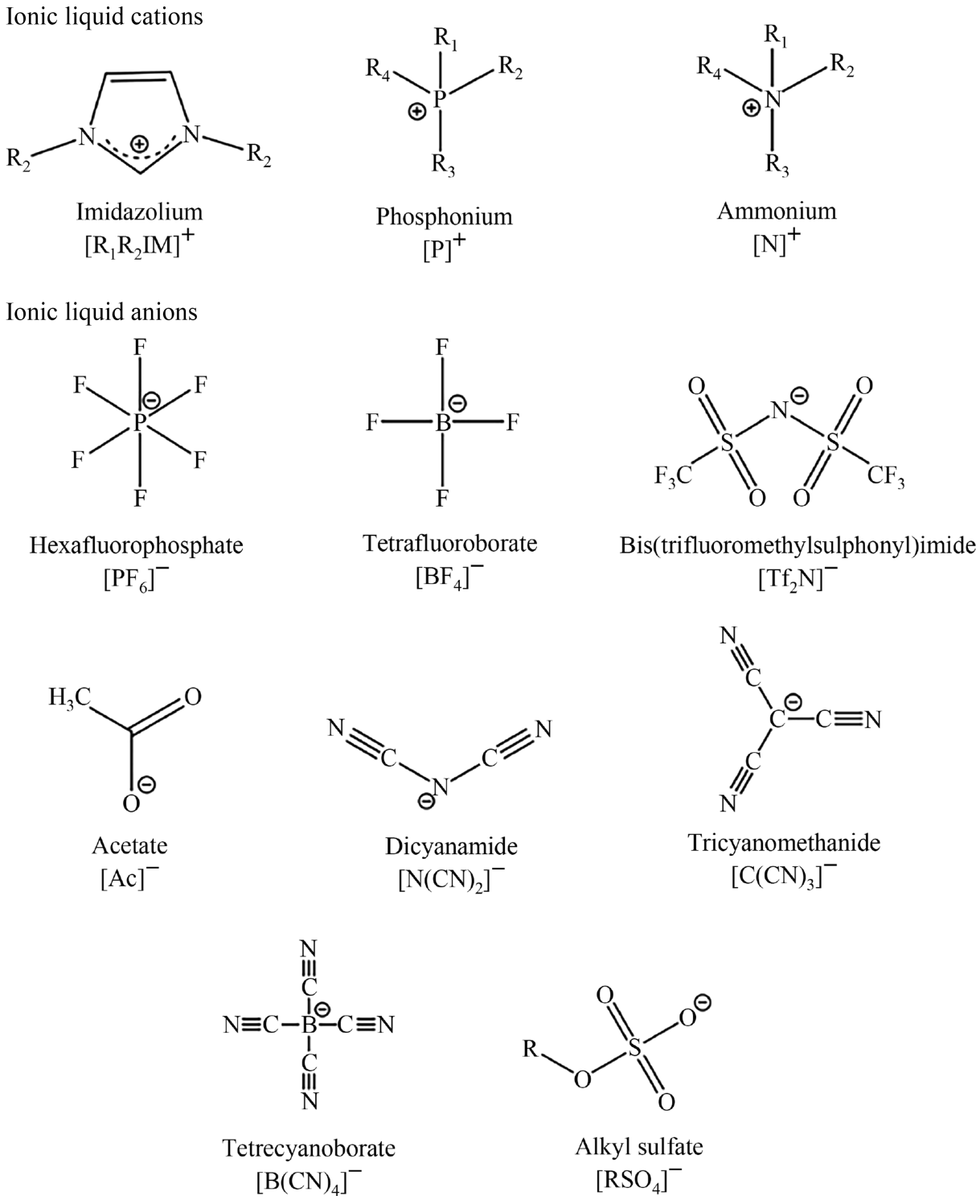


Fig. 12. Most common IL cations and IL anions [121]. Reprinted with permission from Li *et al.*, Copyright 2023, American Chemical Society.

MOF-199, enhancing the adsorption efficiency through synergistic effects [123].

The combination of these two materials offers a promising avenue for optimizing CO_2 adsorption. The combined zeolites and MOFs can lead to synergistic effects that result in enhanced performance. Future research could focus on exploring different combinations of zeolite and MOF types, as well as further investigating the mechanisms underlying the observed improvements in adsorption. Understanding how the interface between the zeolite and MOF affects the adsorption process and how to

precisely control the synthesis conditions to achieve desired properties would be crucial for the development of more efficient adsorbents for CO_2 capture and related applications.

6.7. COF–MOF composite

COFs (covalent organic frameworks) and MOFs are two types of new porous materials. COFs can enhance the mechanical strength of MOFs, making the composite structure more durable and suitable for gas adsorption and separation processes in industrial applications. The combination of COFs and MOFs can provide more chemical functionality [126]. For instance, the material NH_2-UiO-66@Br-COFs, as a core–shell structured hybrid material, not only combines the advantages of MOFs and COFs but also may generate synergistic effects at the MOFs–COFs interface, thereby greatly enhancing the performance of the hybrid material. A unique structure is formed between the NH_2-UiO-66 core and the Br-COFs shell, which can be effectively adjusted by regulating the coating amount of Br-COFs. Compared with NH_2-UiO-66 and Br-COFs, the core–shell interface layer generates a wealth of ultramicro pores, which enhances the CO_2 capacity (169.5 $mg \cdot g^{-1}$ at 273 K and 0.1 MPa) [126], outperforming the corresponding single MOF and COF. The introduction of an abundant nitrogen site in NH_2-UiO-66@Br-COF-4 may be favorable for CO_2 adsorption, as there may be strong acid-base interactions and dipole-quadrupole interactions between the nitrogen site and CO_2 [126].

The successful synthesis of such hybrid materials underscores the potential inherent in combining MOFs and COFs. The presence of covalent linkages, along with the resulting interface characteristics, appears to play a pivotal role in optimizing both porosity and adsorption properties. Future research endeavors could concentrate on exploring additional combinations of MOFs and COFs while investigating the intricate mechanisms that underpin their synergistic interactions. Gaining insights into how various structural and chemical attributes of MOFs and COFs contribute to the overall performance of these hybrids would be invaluable for designing more efficient materials tailored for diverse applications, particularly those about gas adsorption and separation.

7. Selective Adsorption Applications

7.1. Selective adsorption of CO_2/N_2

The selective adsorption of CO_2 over N_2 is determined by the distinctive physical properties of these gases. CO_2 exhibits a smaller kinetic diameter and a larger quadrupole moment in comparison to N_2, thus conferring an enhanced affinity for the surfaces of adsorbent pores. MOFs display a preferential affinity for CO_2 adsorption, setting it apart from other gases. This selectivity is further intensified by the formation of carbon interactions. The inclination for CO_2 within MOFs is attributed to specific interactions, which are contingent upon the dimensions and characteristics of the MOF pores. The pore dimensions and geometry of MOFs enable the selective capture of CO_2 over N_2 due to size exclusion effects. Tailoring pore sizes to correspond with the kinetic diameter of CO_2 can markedly augment its adsorption capacity. Furthermore, the incorporation of functional groups such as basic amines can significantly enhance selectivity for CO_2 over N_2 through acid-base complexation. Unsaturated metal centers in MOFs offer additional adsorption sites for CO_2 *via* coordination bonds, which are not accessible to N_2. Certain MOFs display flexibility, allowing structural alterations in response to gas adsorption. This breathing effect may augment selectivity for CO_2 over N_2 employing preferential adsorption coupled with subsequent structural modifications that promote further uptake of CO_2. Additionally, MOFs with hydrophobic surfaces may preferentially adsorb CO_2 over N_2, given that CO_2 demonstrates greater solubility in non-polar environments compared to N_2 [127].

Valenzano *et al.* [128] conducted investigations into the adsorption behavior of diverse gases on Mg-MOF-74. The disparities in adsorption enthalpy provide indicators of adsorption capacity and constitute a potent tool for separation. The enhanced interaction can elevate the affinity for CO_2, thereby advancing selectivity in comparison to molecules with weaker adsorbate-framework interactions. Banerjee *et al.* [19] indicated that ZIF-78 exhibits a high affinity and capacity for CO_2. ZIF-78 displays a CO_2 adsorption capacity fourfold greater than that of CH_4 and eight to ten times higher than O_2 and N_2 [19]. Li *et al.* [80] developed MOFs with a core–shell architecture, including MOF-11 (acetate), MOF-12 (propionate), MOF-13 (butyrate), and MOF-14 (valerate). The monocarboxylates affect gas adsorption characteristics as well as hydrophilicity. An extension in alkyl chain length leads to a decrease in CO_2 adsorption capacity, however, it enhances both CO_2/N_2 selectivity and hydrophilic stability. Of these compounds, MOF-11 (acetate) exhibits the highest CO_2 adsorption capacity but suffers from lower hydrophilic stability; in contrast, MOF-14 (valerate) demonstrates significant CO_2 adsorption selectivity and robust hydrophilic stability in CO_2/N_2 binary mixtures. Hence, the researchers integrated MOF-11 with MOF-14, achieving excellent hydrophilic stability by encasing a MOF-11 core within a MOF-14 shell. In this structure, the MOF-11 core promotes effective CO_2 capture, whereas the MOF-14 outer layer acts both as a nitrogen sieve and a hydrophobic protective barrier. Despite these improvements, existing literature identifies several limitations [19,80]. For example, the adsorption enthalpy measurements for CO_2 on Mg-MOF-74 suggest a predominantly physical adsorption mechanism, indicating reversibility, which may compromise the stability of the adsorbed CO_2 [128].

Furthermore, although ZIF-78 shows high CO_2 affinity and selectivity over N_2, functional groups such as $-NO_2$ and $-CN$ that enhance selectivity may also introduce challenges in MOF synthesis and potential stability issues [19]. Researchers have synthesized a novel MOF designated as [Cu(bcppm)H_2O], which has demonstrated exceptional performance in the selective separation of CO_2/N_2 through post-synthetic structural modification. During activation, [Cu(bcppm)H_2O] transformed from a two-dimensional to a three-dimensional structure with a concurrent reduction in pore size, as examined *via* single-crystal and powder XRD analyses. The reduction in pore size to approximately 0.36 nm renders it highly suitable for size-selective CO_2/N_2 separation, with precise pore size control achieved through post-synthetic treatment [129].

Prospective strategies for enhancing selective CO_2 adsorption in preference to N_2 ought to concentrate on MOFs with customized pore sizes and functionalities that optimize CO_2 interactions while reducing N_2 adsorption. Core–shell structures, exemplified by those synthesized by Li *et al.* [80], present a promising methodology by integrating elevated CO_2 adsorption capacity with selectivity and hydrophilic stability. Subsequent research must investigate the impacts of varying alkyl chain lengths on adsorption properties and stability, as well as foster the development of MOFs with superior hydrolytic stability to sustain performance under humid conditions. Computational modeling and experimental validation are critical in optimizing material performance and separation processes. Table 2 summarizes the performance data of MOFs in terms of CO_2 adsorption, covering key indicators such as adsorption conditions, adsorption capacity, selectivity coefficient, and cycling performance. These materials exhibit diverse performances under different conditions, providing important references for the material selection and optimization of CO_2 capture technologies.

Table 2
Comparison of selective adsorption performance of MOFs for CO_2/N_2.

Materials type	Adsorption conditions	Adsorption capacity/mmol·g^{-1}	Selection coefficient	Number of cycles/cycling stability	Reference
ZIF-8/GONR	n.a.	n.a.	19.3	Recyclable	[130]
PEI-ZIF-8	298 K, 0.1 MPa	1.2	49	Recyclable	[131]
AEEA-ZIF-8	298 K, 0.1 MPa	3.6	n.a.	7/95%	[132]
45PEI@ZIF-8	338 K, 0.1 MPa	1.6	62	n.a.	[133]
15TETA/ZIF-8	298 K, 0.1 MPa	2.7	n.a.	Reduced performance in recycling	[134]
ED-ZIF-8	298 K, 0.1 MPa	3	23	4/98%	[135]
ZIF-modified biochar	298 K, 0.1 MPa	3.0	38.6	10/96%	[136]
M-101-mXDA	298 K, 0.1 MPa	>1	>100	4/recyclable	[137]
Cellulose diacetate-SiO_2-NH_2-UiO-66	333 K, 0.1 MPa	2.5	18.12	45/recyclable	[138]
NH_2-MIL-101(Cr) membranes	n.a.	n.a.	37	50/recyclable	[139]
HKUST-1	298 K, 0.1 MPa	4.71	89.1	6/recyclable	[127]
IL@HUiO2:1 MMM	n.a.	n.a.	21.5	Recyclable	[140]
RC-ML-1	298 K, 0.1 MPa	25.79	n.a.	6/recyclable	[141]
SU−102−Na	298 K, 0.1 MPa	2	576.8	5/recyclable	[142]
DES-2@MOF-808-FR	298 K, 0.1 MPa	4.16	1184	10/91.2%	[5]
F@MOF-808	298 K, 0.1 MPa	1.97	28	10/recyclable	[143]

Note: ZIF-8/GONR (ZIF-8/graphene nanoribbon hybrid nanoplates), PEI-ZIF-8 (polyethyleneimine functionalized ZIF-8), AEEA-ZIF-8 (aminoethylethanolamine functionalized porous ZIF-8 nanoparticles), ED-ZIF-8 (ethylenediamine-ZIF-8), M-101-mXDA (0.3) (Cr-based MOF-*m*-xylylenediamine), IL@HUiO2:1 MMM (ionic liquid membranes@defective UiO-66-NH_2 with high defect concentration), SU-102-Na (SU-102 mixed with NaCl), DES-2@MOF-808-FR (2 representative the mass ratio of DES to MOF-808 and FR (the formate ligand removed)), F@MOF-808 (fluoride-rich MOF-808).

7.2. Selective adsorption of CO_2/H_2O

Most sorbents demonstrate substantial CO_2 uptake from unsaturated metal centers or extensive surface areas. However, the presence of moisture introduces competitive adsorption dynamics, causing a reduction in CO_2 capture efficacy within humid flue gases. The differential adsorptive affinity for CO_2 as opposed to H_2O depends on the intensity of interactions between these molecules and the active sites of the adsorbent. In practical adsorptive systems, CO_2 and H_2O are concurrently present at the interface of solid and gas phases, whereby their adsorption may occur either simultaneously or separately. The extent of adsorption is determined by the affinity of the gas molecules for the adsorbent, with the more strongly interacting species presenting higher adsorptive quantities. Since the dipole moment of H_2O is greater than that of the CO_2 molecule, H_2O molecules interact more strongly with the adsorbent surface. This interaction displaces the cations of the adsorbent structure from the framework, fixing them at the center of the pores of the adsorbent and thereby inhibiting CO_2 molecules from occupying the adsorption sites.

The primary advantage of a core−shell structure is its ability to protect the core material from external interference [144]. The Mg-MOF-74@ZIF-8 composite features Mg-MOF-74 as the core, enveloped within the hydrophobic shell of ZIF-8 to enhance stability. The study examined how variations in the number of ZIF-8 layers affect the morphology of the composite, structural attributes, hydrophobicity, and CO_2 adsorption performance. Findings indicated an increase in hydrophobicity with the addition of ZIF-8 layers [145]. Yang and colleagues [146] developed a novel core−shell structured material. The synthesized LiX@ZIF-8 nanoparticles were purified using deionized water. The core−shell configuration provided the LiX@ZIF-8 nanoparticles with intermediate hydrophobic properties, acting as a bridge between those of 13X and ZIF-8. Dynamic testing evaluated the CO_2 adsorptive capacity and stability of the composite, revealing a significant enhancement in CO_2 adsorption under 50% relative humidity [146]. Yu and Balbuena [147] introduced bromine-based moieties to augment the hydrophobic properties of MOF. This strategic modification effectively mitigated competitive water molecule adsorption, thereby maintaining the CO_2 capture efficiency of the material in humid environments [147]. By integrating hydrophobic functional groups, such as bromide groups, the hydrophobic characteristics of MOFs can be enhanced. This reduces the competitive adsorption of water molecules, thus preserving the CO_2 capture efficiency of the material under humid conditions. Yu and Balbuena [147] demonstrated that the adsorption of CO_2 by the $-NH_2$ and −OH functional groups-modified UiO-66(Zr) decreased in the presence of water, whereas the hydrophobicity of the −Br functional group had a minimal effect on CO_2 adsorption in the presence of water.

Coating technology constitutes a method for enhancing selective adsorption efficacy. Jin *et al.* [148] addressed this by applying polydimethylsiloxane coating to Mg-MOF-74, which augmented its resistance to moisture and increased CO_2 adsorption under humid conditions. The resultant M74@P sample exhibited superior performance, retaining 6.65 mmol·g^{-1} of CO_2 from a CO_2/N_2 mixture across 100 cycles, surpassing the 1.17 mmol·g^{-1} achieved by unmodified Mg-MOF-7. Variations in adsorptive environments significantly affect the CO_2 capture efficiency of MOFs. Xian *et al.* [149] examined the influence of water vapor on MOF performance in CO_2/CH_4 mixtures. Their findings indicate that MIL-100(Fe) enhanced the selective adsorption of CO_2/CH_4 in the presence of water vapor, attributed to the hydrolysis of the ferrous oxygen group and the formation of functional −OH alkaline surfaces that facilitate interaction with acidic CO_2. Conversely, the selective adsorption of CO_2/CH_4 by MIL-101(Cr) was reduced due to water vapor competing with CO_2 and occupying adsorption sites [149].

Researchers have improved the reusability and stability of MOF adsorbents in humid conditions through a post-synthetic modification method involving the reaction of epoxides with diamine groups. Specifically, the modified adsorbent N-ethyl ethylenediamine-MOF/Al-Si-C17-200 (een-MOF/Al-Si-C17-200) exhibits significant hydrophobicity, which can hinder the diffusion of water vapor through the pores [150]. Fig. 13 displays the performance comparison between een-MOF/Al-Si-C17-200 and een-MOF/Al-Si, where een represents N-ethyl ethylenediamine [150].

Two series of amine-functionalized zirconium MOFs (MOF-808) have been developed by researchers, with post-synthetic modifications to integrate amino acids or polyamines. These materials have demonstrated superior efficacy in the direct air capture of CO_2 [151]. Fig. 14 depicts a modification of MOF-808. For MOF-808-AA (AA = amino acids), amino acids were introduced into the MOF-808 framework through the coordination of Zr(IV) with carboxylate groups. For MOF-808-PA, 3-chloropropionic acid was first coordinated with Zr(IV) of MOF-808, and then polyamines were covalently incorporated into the structure *via*

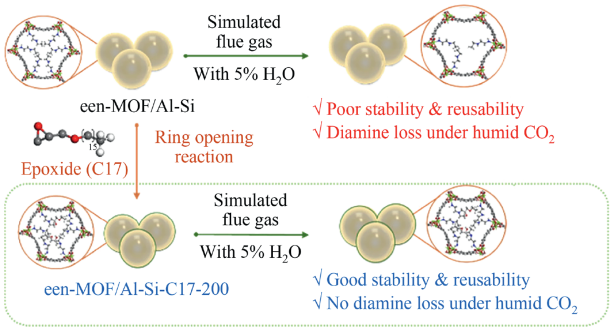


Fig. 13. Comparison between een-MOF/Al-Si-C17-200 and een-MOF/Al-Si; een = *N*-ethyl ethylenediamine [150]. Reprinted with permission from Choe *et al.* Copyright 2022, American Chemical Society.

nucleophilic substitution reactions. Under dry conditions, a covalent interaction occurs with the amine groups in MOF-808-AA and MOF-808-PA to form carbamic acid or carbamate. Water promotes the reaction between amine groups and CO_2 to form bicarbonate species.

In practical applications, the selective adsorption capacity of MOFs is essential for the effective separation of gas mixtures, including natural gas purification, industrial exhaust gas treatment, and air purification. By designing and synthesizing MOFs with specific adsorption properties, tailored solutions for various gas separation applications can be provided. Additionally, the cyclic stability and recovery capacity of MOFs during gas adsorption and separation processes are crucial determinants of their applicability in real-world scenarios. Researchers continue to investigate innovative materials design and synthetic strategies to enhance MOF performance, reduce production costs, and thereby promote the commercialization of MOFs in the domain of gas adsorption and separation.

7.3. Selective adsorption of CO_2/CH_4

The preferential adsorption of CO_2 over CH_4 is of paramount importance in various industrial applications, particularly in the purification of natural gas. CO_2, characterized by a linear and polar structure with a quadrupole moment, differs significantly from the nonpolar, tetrahedral structure of CH_4. These differences in polarity influence their respective affinities for adsorbent surfaces. It is crucial to enhance adsorptive selectivity by incorporating nitrogen-rich functional groups that preferentially interact with CO_2, thereby improving the separation of CO_2 and CH_4 in mixed gas streams. The incorporation of nitrogen-rich functional groups into MOFs enhances the affinity for CO_2, which in turn improves the selectivity of CO_2 over CH_4. The introduction of amino groups into MIL-53(Al) has been shown to significantly increase its CO_2 adsorption capacity, resulting in enhanced selectivity for CO_2 over CH_4 [50]. Researchers modified the microporous isoreticular MOF-3 (IRMOF-3) with AMP (aminomethyl propanol) to create AMP@IRMOF-3, which demonstrated improved CO_2/CH_4 adsorption selectivity [152].

Enhancing the electrostatic interactions between MOFs and CO_2 is a key to improving the selective adsorption of CO_2. MOF-177, with its multidimensional structure, was synthesized and evaluated for CO_2 and CH_4 adsorption, with static adsorption analyses attributing the enhanced CO_2 affinity to pronounced electrostatic interactions [153]. New ZIF materials infused with chlorine atoms, termed COK-17, display an extraordinarily high affinity for CO_2 adsorption. COK-17 optimizes CO_2 adsorption through chlorine atoms and amplifies London dispersion forces, achieving high selectivity in the adsorption-based separation of CO_2 and CH_4 [55]. The MOF Co(bdp) (bdp^{2-} = 1,4-benzenedipyrazolate) is capable of nearly complete exclusion of CH_4, and selective adsorption of CO_2 from a 50:50 CO_2/CH_4 mixture. The selectivity of Co(bdp) for CO_2 over CH_4 derives from a reversible guest templating mechanism, wherein the framework expands upon CO_2 adsorption and reverts to its non-templated phase post-adsorption. Such reversible structural adaptations enable the framework to modify pore sizes at varying gas pressures, selectively adsorption of CO_2, and obstruct CH_4. The pore size of Co(bdp) closely matches the diameter of a CO_2 molecule, whereas the CH_4 molecule is marginally larger, thereby inhibiting CH_4 entry post-framework expansion. The thermodynamic properties of CO_2 adsorption confer greater stability within the framework, as CO_2 adsorption enthalpy significantly exceeds that of CH_4, prompting the framework to preferentially adsorb CO_2 over CH_4 under equivalent conditions [154].

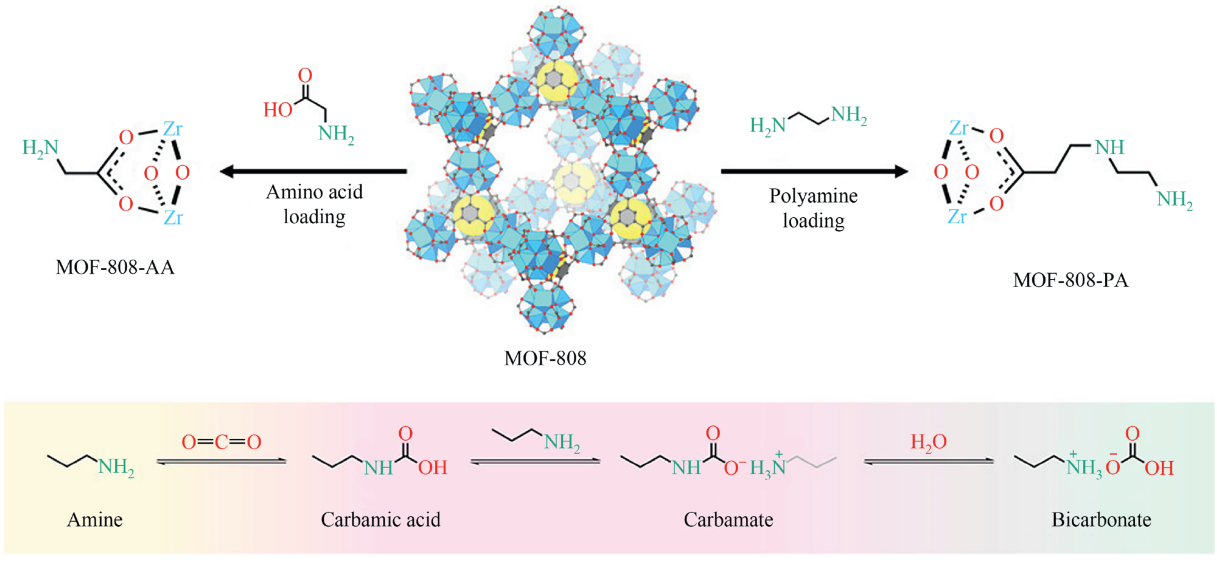


Fig. 14. Two-step modification of MOF-808 and its adsorption mechanism of CO_2 [151]. Reprinted with permission from Chen *et al.*, Copyright 2024, American Chemical Society.

8. Commercial Application of MOFs

The commercial scalability of MOFs remains constrained by high production costs, necessitating optimized synthesis routes and industrial-scale processes to improve economic viability. Key factors influencing cost include raw materials (particularly expensive organic ligands) as well as solvents, equipment, and market demand. While conventional metal salts like nitrates and chlorides pose safety and corrosion challenges, industrial production often employs cheaper alternatives such as $AlCl_3 \cdot 6H_2O$ or $Al_2(SO_4)_3 \cdot 18H_2O$ for aluminum-based MOFs, where moderate impurity levels can be tolerated without significantly compromising structural integrity [155]. Ligand cost is a major driver of expense, though waste-upcycling strategies might offer a promising path to reduce material costs [156]. Solvent selection also critically influences both cost and environmental impact; traditional solvents like DMF are toxic and energy-intensive to remove, whereas green alternatives (*e.g.*, water or ethanol) enable more sustainable and economical synthesis, as demonstrated in the kilogram-scale production of MOF-303(Al) or ZIF-8 in ethanol [155,157]. Advances in synthesis methods, including microwave-assisted reactions, continuous flow systems, mechanochemical synthesis, and seed-mediated growth [158], have substantially improved space-time yields, reduced reaction times, and lowered energy consumption [159].

The scalability and stability of MOFs under realistic conditions are critical for industrial implementation. A prominent example is CALF-20, which has been successfully scaled to hundreds of tons annually through the collaboration between BASF and Svante [160]. This material has been granulated into robust pellets that maintain structural integrity and adsorption capacity under industrial handling conditions. Notably, CALF-20 demonstrates exceptional performance in actual flue gas environments. In 2023, it was deployed at a cement plant in Richmond, Canada, where it continuously captures approximately 1 ton of CO_2 per day from complex, wet, and acidic flue gas streams [160]. The material exhibits remarkable stability in the presence of moisture and impurities, achieving high CO_2 selectivity under realistic pressure swing adsorption conditions.

Through optimized production processes, Svante has reduced the manufacturing cost of CALF-20 to approximately $1 per gram, with projections to further decrease expenses. Pilot tests in coal-fired power and cement plants indicate that the CO_2 capture cost can be maintained at $30–80 per ton [7]. This successful integration of scalable production, granulation technology, and demonstrated performance in industrial flue gas treatment establishes CALF-20 as a leading candidate for widespread carbon capture applications.

Despite these advances, MOFs remain costlier than conventional adsorbents (*e.g.*, zeolites or activated carbon), underscoring the need for continued innovation in scalable and low-cost manufacturing to broaden industrial applicability. To advance the commercialization of MOFs, it is imperative to optimize the synthesis processes from laboratory-scale to industrial-scale production, thereby reducing costs. The cost of MOFs production is affected by multiple factors, including raw materials, solvents, equipment, production scale, as well as market factors. To reduce the production cost of MOFs, comprehensive optimization is needed in these aspects.

9. Conclusion and Outlook

This review has systematically examined the rational design of MOF for enhanced CO_2 capture, addressing the fundamental mechanisms and advanced strategies to overcome the challenges of CO_2 adsorption capacity, selectivity, and stability. The CO_2 adsorption mechanism in MOFs involves both physisorption, dominated by van der Waals forces within the pores, and chemisorption, which entails chemical interactions such as the formation of coordination bonds or carbamates with metal sites or amine-functionalized groups. Key performance-enhancement strategies discussed include precise pore size and morphology optimization, surface functionalization (*e.g.*, introducing amine groups), defect engineering, and the formation of composite materials (*e.g.*, with polymers or carbonaceous substances).

Despite significant laboratory advances, the path to industrial-scale application requires overcoming several critical hurdles. For instance, computational methods like DFT, Grand Canonical Monte Carlo, and machine learning are indispensable for the high-throughput screening and virtual design of MOFs, significantly reducing the need for extensive trial-and-error experimentation. A primary challenge remains improving the accuracy of these models to predict performance under real-world, multi-component gas conditions. The future lies in developing a closed-loop, intelligent design pipeline where computational predictions directly guide automated synthesis and testing, dramatically accelerating the discovery of novel, high-performance adsorbents. For industrial viability, MOFs must exhibit not only high capacity but also excellent hydrolytic and mechanical stability over thousands of adsorption-desorption cycles.

Accordingly, the journey from conceptual MOF design to a commercially viable CO_2 capture technology is challenging but attainable. It demands a highly interdisciplinary approach, integrating computational modeling, sophisticated synthesis, advanced characterization, and rigorous engineering under realistic conditions. It is believed that by focusing on the key areas of stability, selectivity, scalability, and sustainability, the next generation of MOF adsorbents can play a transformative role in global carbon mitigation efforts.

CRediT Authorship Contribution Statement

Wanyi Zeng: Writing – original draft, Methodology, Formal analysis, Conceptualization. Minzhong Huang: Writing – review & editing, Methodology. Bin Chen: Writing – review & editing. Kok Bing Tan: Writing – review & editing. Dongren Cai: Writing – review & editing. Wanchai Pluempanupat: Writing – review & editing. Guowu Zhan: Writing – review & editing, Supervision, Funding acquisition.

Data Availability

No primary research results, software, or code have been included, and no new data were generated or analyzed as part of this review.

Declaration of Competing Interest

The authors declare that they have no known competing financial interests or personal relationships that could have appeared to influence the work reported in this paper.

Acknowledgements

This work was financially supported by the National Natural Science Foundation of China (22322806 and 22350410389). Additionally, we express gratitude to the Postdoc Innovative Funds (605-50Y24020).

References

[1] E. Soroush, M. Mesbah, N. Hajilary, M. Rezakazemi, ANFIS modeling for prediction of CO_2 solubility in potassium and sodium based amino acid salt solutions, *J. Environ. Chem. Eng.* 7 (1) (2019) 102925.

[2] Z.H. Liang, Y.Y. Ou, E.M. El-Sayed, K.Z. Su, W.J. Wang, D.Q. Yuan, Effect of functional groups on low-concentration carbon dioxide capture in UiO-66-type metal–organic frameworks, *Inorg. Chem.* 62 (21) (2023) 8309–8314.

[3] R.J. Ciora, B. Sengupta, F. Wang, S.G. Li, M. Yu, Direct modification of pelletized 13X zeolite by atomic layer deposition toward effective CO_2 capture from flue gas, *Chem. Eng. J.* 497 (2024) 154733.

[4] H.Q. Yang, Z.H. Xu, M.H. Fan, R. Gupta, R.B. Slimane, A.E. Bland, I. Wright, Progress in carbon dioxide separation and capture: a review, *J. Environ. Sci.* 20 (1) (2008) 14–27.

[5] X.Q. Zhang, D.Y. Zhang, C. Zhang, R.J. Ma, X.C. Zhu, L.W. Wang, Enhancing CO_2 solubility for efficient carbon capture *via* self-assembly deep eutectic solvents on MOF-808, *Sep. Purif. Technol.* 358 (2025) 130331.

[6] M.Z. Zheng, Z. Fang, W.J. Xue, T.A. Yan, H.L. Huang, C.L. Zhong, CO_2 chemical trap and electronegative microenvironment enable metal–organic framework with one-step ethylene purification from quaternary mixture, *Adv. Funct. Mater.* 35 (25) (2025) 2422135.

[7] J.B. Lin, T.T.T. Nguyen, R. Vaidhyanathan, J. Burner, J.M. Taylor, H. Durekova, F. Akhtar, R.K. Mah, O. Ghaffari-Nik, S. Marx, N. Fylstra, S.S. Iremonger, K.W. Dawson, P. Sarkar, P. Hovington, A. Rajendran, T.K. Woo, G.K.H. Shimizu, A scalable metal–organic framework as a durable physisorbent for carbon dioxide capture, *Science* 374 (6574) (2021) 1464–1469.

[8] S.Q. Meng, X.Q. Ju, J.W. Wang, B.L. Cui, Y.X. Liu, H.S. Ma, D.C. Wang, Z.Y. Yang, Development of efficient CO_2 adsorbents: synthesis and performance evaluation of dopamine-modified halloysite nanotubes loaded with ZIF-8, *Sep. Purif. Technol.* 357 (2025) 130179.

[9] X. Feng, H.S. Jena, C. Krishnaraj, D. Arenas-Esteban, K. Leus, G.B. Wang, J.M. Sun, M. Rüscher, J. Timoshenko, B. Roldan Cuenya, S. Bals, P. van der Voort, Creation of exclusive artificial cluster defects by selective metal removal in the (Zn, Zr) mixed-metal UiO-66, *J. Am. Chem. Soc.* 143 (51) (2021) 21511–21518.

[10] H.J. Zhao, J.L. Dong, S.J. Chen, H. Wang, G.D. Zhao, Metal–organic frameworks and their composites for carbon dioxide capture: recent advances and challenges, *Fuel* 378 (2024) 132973.

[11] W.L. Li, Q. Shuai, J.M. Yu, Recent advances of carbon capture in metal–organic frameworks: a comprehensive review, *Small* 20 (45) (2024) e2402783.

[12] C.A. Trickett, A. Helal, B.A. Al-Maythalony, Z.H. Yamani, K.E. Cordova, O.M. Yaghi, The chemistry of metal–organic frameworks for CO_2 capture, regeneration and conversion, *Nat. Rev. Mater.* 2 (2017) 17045.

[13] J.H. Choe, H. Kim, C.S. Hong, MOF-74 type variants for CO_2 capture, *Mater. Chem. Front.* 5 (14) (2021) 5172–5185.

[14] H.F. An, W.J. Tian, X. Lu, H.M. Yuan, L.Y. Yang, H. Zhang, H.M. Shen, H. Bai, Boosting the CO_2 adsorption performance by defect-rich hierarchical porous Mg-MOF-74, *Chem. Eng. J.* 469 (2023) 144052.

[15] K.S. Park, Z. Ni, A.P. Côté, J.Y. Choi, R.D. Huang, F.J. Uribe-Romo, H.K. Chae, M. O'Keeffe, O.M. Yaghi, Exceptional chemical and thermal stability of zeolitic imidazolate frameworks, *Proc. Natl. Acad. Sci. USA* 103 (27) (2006) 10186–10191.

[16] H. Hayashi, A.P. Côté, H. Furukawa, M. O'Keeffe, O.M. Yaghi, Zeolite A imidazolate frameworks, *Nat. Mater.* 6 (7) (2007) 501–506.

[17] R. Banerjee, A. Phan, B. Wang, C. Knobler, H. Furukawa, M. O'Keeffe, O.M. Yaghi, High-throughput synthesis of zeolitic imidazolate frameworks and application to CO_2 capture, *Science* 319 (5865) (2008) 939–943.

[18] B. Wang, A.P. Côté, H. Furukawa, M. O'Keeffe, O.M. Yaghi, Colossal cages in zeolitic imidazolate frameworks as selective carbon dioxide reservoirs, *Nature* 453 (7192) (2008) 207–211.

[19] R. Banerjee, H. Furukawa, D. Britt, C. Knobler, M. O'Keeffe, O.M. Yaghi, Control of pore size and functionality in isoreticular zeolitic imidazolate frameworks and their carbon dioxide selective capture properties, *J. Am. Chem. Soc.* 131 (11) (2009) 3875–3877.

[20] N. Klomkliang, N. Threerattanakulpron, W. Wongsombat, P. Phadungbut, S. Chaemchuen, S. Supasitmongkol, J. Serafin, L.F. Herrera Diaz, Experimental and molecular simulation study of CO_2 adsorption in ZIF-8: atomic heat contributions and mechanism, *J. Ind. Eng. Chem.* 145 (2025) 831–841.

[21] Y.C. Lin, C.L. Kong, L. Chen, Direct synthesis of amine-functionalized MIL-101(Cr) nanoparticles and application for CO_2 capture, *RSC Adv.* 2 (16) (2012) 6417.

[22] G. Férey, C. Mellot-Draznieks, C. Serre, F. Millange, J. Dutour, S. Surblé, I. Margiolaki, A chromium terephthalate-based solid with unusually large pore volumes and surface area, *Science* 309 (5743) (2005) 2040–2042.

[23] Z.Q. Wang, S.M. Cohen, Modulating metal–organic frameworks to breathe: a postsynthetic covalent modification approach, *J. Am. Chem. Soc.* 131 (46) (2009) 16675–16677.

[24] S. Bourrelly, P.L. Llewellyn, C. Serre, F. Millange, T. Loiseau, G. Férey, Different adsorption behaviors of methane and carbon dioxide in the isotypic nanoporous metal terephthalates MIL-53 and MIL-47, *J. Am. Chem. Soc.* 127 (39) (2005) 13519–13521.

[25] A. Celeste, P. Fertey, J.P. Itié, G. Blanita, C. Zlotea, F. Capitani, Exploring the role of ligand connectivity in MOFs mechanical stability: the case of MIL-100(Cr), *J. Am. Chem. Soc.* 146 (13) (2024) 9155–9162.

[26] J.H. Cavka, S. Jakobsen, U. Olsbye, N. Guillou, C. Lamberti, S. Bordiga, K.P. Lillerud, A new zirconium inorganic building brick forming metal organic frameworks with exceptional stability, *J. Am. Chem. Soc.* 130 (42) (2008) 13850–13851.

[27] M.D. Ma, A.N. Zhou, T. Hong, X.Y. Jia, M.X. Liu, Tailored porous structure and CO_2 adsorption capacity of Mg-MOF-74 *via* solvent polarity regulation, *Chem. Eng. J.* 476 (2023) 146845.

[28] R. Oktavian, R. Goeminne, L.T. Glasby, P. Song, R. Huynh, O.T. Qazvini, O. Ghaffari-Nik, N. Masoumifard, J.L. Cordiner, P. Hovington, V. van Speybroeck, P.Z. Moghadam, Gas adsorption and framework flexibility of CALF-20 explored *via* experiments and simulations, *Nat. Commun.* 15 (1) (2024) 3898.

[29] Z. Chen, C.H. Ho, X.L. Wang, S.M. Vornholt, T.M. Rayder, T. Islamoglu, O.K. Farha, F. Paesani, K.W. Chapman, Humidity-responsive polymorphism in CALF-20: a resilient MOF physisorbent for CO_2 capture, *ACS Mater. Lett.* 5 (11) (2023) 2942–2947.

[30] J. Drwęska, F. Formalik, K. Roztocki, R.Q. Snurr, L.J. Barbour, A.M. Janiak, Unveiling temperature-induced structural phase transformations and CO_2 binding sites in CALF-20, *Inorg. Chem.* 63 (41) (2024) 19277–19286.

[31] X.Y. Wang, Z. Zhang, W.Q. Huang, X.F. Li, B.Y. Yan, Preparation of highly water stable HKUST-1@Pyr composites for excellent CO_2 capture capability and efficient separation of CO_2/N_2, *Inorg. Chem. Commun.* 156 (2023) 111252.

[32] Ü. Kökçam-Demir, A. Goldman, L. Esrafili, M. Gharib, A. Morsali, O. Weingart, C. Janiak, Coordinatively unsaturated metal sites (open metal sites) in metal–organic frameworks: design and applications, *Chem. Soc. Rev.* 49 (9) (2020) 2751–2798.

[33] X.F. Li, H. Bian, W.Q. Huang, B.Y. Yan, X.Y. Wang, B. Zhu, A review on anion-pillared metal–organic frameworks (APMOFs) and their composites with the balance of adsorption capacity and separation selectivity for efficient gas separation, *Coord. Chem. Rev.* 470 (2022) 214714.

[34] L.F. Yang, X.L. Cui, Y.B. Zhang, Q.J. Wang, Z.Q. Zhang, X. Suo, H.B. Xing, Anion pillared metal–organic framework embedded with molecular rotors for size-selective capture of CO_2 from CH_4 and N_2, *ACS Sustainable Chem. Eng.* 7 (3) (2019) 3138–3144.

[35] K. Forrest, T. Pham, S.K. Elsaidi, M.H. Mohamed, P.K. Thallapally, M.J. Zaworotko, B. Space, Investigating CO_2 sorption in SIFSIX-3-M (M = Fe, Co, Ni, Cu, Zn) through computational studies, *Cryst. Growth Des.* 19 (7) (2019) 3732–3743.

[36] K. Suresh, D. Aulakh, J. Purewal, D.J. Siegel, M. Veenstra, A.J. Matzger, Optimizing hydrogen storage in MOFs through engineering of crystal morphology and control of crystal size, *J. Am. Chem. Soc.* 143 (28) (2021) 10727–10734.

[37] G. Lee, I. Ahmed, S.H. Jhung, CO_2 adsorption using functionalized metal–organic frameworks under low pressure: contribution of functional groups, excluding amines, to adsorption, *Chem. Eng. J.* 481 (2024) 148440.

[38] I. Akiyama, T. Kato, S. Kannaka, A. Ito, M. Ohtani, Effect of boron-doping on gate-opening CO_2 adsorption in zinc-benzimidazolate coordination networks, *ACS Appl. Mater. Interfaces* 16 (19) (2024) 24816–24822.

[39] G. Lee, S.H. Jhung, CO_2 capture using functionalized MIL-101(Cr) metal–organic frameworks: functionality nanoarchitectonics of nanospace for CO_2 adsorption, *Sep. Purif. Technol.* 354 (2025) 129514.

[40] J. Amesimeku, Y.C. Zhao, K. Li, J.L. Gu, Rapid synthesis of hierarchical cerium-based metal organic frameworks for carbon dioxide adsorption and selectivity, *Microporous Mesoporous Mater.* 359 (2023) 112658.

[41] T.K. Vo, V.C. Nguyen, D.T. Quang, B.J. Park, J. Kim, Formation of structural defects within UiO-66(Zr)-$(OH)_2$ framework for enhanced CO_2 adsorption using a microwave-assisted continuous-flow tubular reactor, *Microporous Mesoporous Mater.* 312 (2021) 110746.

[42] C.Q. Fan, J. Xu, H. Jiang, R.Z. Chen, Controllable synthesis of hollow ZIF-8 microspheres *via* interface reaction with enhanced CO_2 adsorption, *J. Solid State Chem.* 309 (2022) 123017.

[43] S.R.D. Raveendran, L.P. Teh, R. Othaman, C.H. Chia, Enhanced carbon dioxide adsorption performance of UiO-66-SO_3H with a mixed ligand strategy, *J. Environ. Chem. Eng.* 12 (5) (2024) 113404.

[44] S. Mutyala, M. Jonnalagadda, S.M. Ibrahim, Effect of modification of UiO-66 for CO_2 adsorption and separation of CO_2/CH_4, *J. Mol. Struct.* 1227 (2021) 129506.

[45] M.G. Shang, J. Zhang, J.Q. Sun, S.M. Yu, F. Hua, X.X. Xuan, X. Sun, S. Filatov, X. B. Yi, Amine-functionalized mesoporous UiO-66 aerogel for CO_2 adsorption, *Chin. J. Chem. Eng.* 54 (2023) 36–43.

[46] K. Pirzadeh, K. Esfandiari, A.A. Ghoreyshi, M. Rahimnejad, CO_2 and N_2 adsorption and separation using aminated UiO-66 and $Cu_3(BTC)_2$: a comparative study, *Kor. J. Chem. Eng.* 37 (3) (2020) 513–524.

[47] S. Mutyala, Y.D. Yu, W.G. Jin, Z.S. Wang, D.Y. Zheng, C.R. Ye, B.B. Luo, CO_2 capture using amine incorporated UiO-66 in atmospheric pressure, *J. Porous Mater.* 26 (6) (2019) 1831–1838.

[48] N.C. Pham, T.K. Vo, Q.B. Nguyen, T.K. Nguyen, T.H.C. Nguyen, N.N. Dao, J. Kim, V.C. Nguyen, Ethylenediamine-entrapped defective UiO-66(Zr) frameworks for improved CO_2 adsorption and selectivity, *Inorg. Chem. Commun.* 158 (2023) 111476.

[49] Z. Li, W.Z. Sun, C. Chen, Q.R. Guo, X. Li, M.W. Gu, N.J. Feng, J. Ding, H. Wan, G. F. Guan, Deep eutectic solvents appended to UiO-66 type metal organic frameworks: preserved open metal sites and extra adsorption sites for CO_2 capture, *Appl. Surf. Sci.* 480 (2019) 770–778.

[50] S. Couck, J.F.M. Denayer, G.V. Baron, T. Rémy, J. Gascon, F. Kapteijn, An amine-functionalized MIL-53 metal–organic framework with large separation power for CO_2 and CH_4, *J. Am. Chem. Soc.* 131 (18) (2009) 6326–6327.
[51] D. Britt, H. Furukawa, B. Wang, T.G. Glover, O.M. Yaghi, Highly efficient separation of carbon dioxide by a metal–organic framework replete with open metal sites, *Proc. Natl. Acad. Sci. USA* 106 (49) (2009) 20637–20640.
[52] S.S.Y. Chui, S.M.F. Lo, J.P.H. Charmant, A.G. Orpen, I.D. Williams, A chemically functionalizable nanoporous material $[Cu_3(TMA)_2(H_2O)_3]_n$, *Science* 283 (5405) (1999) 1148–1150.
[53] X.Y. Lin, W.P. Zeng, M.Y. Liu, Q.H. Zhong, T. Su, L.Z. Gong, Y.M. Liu, Amino-modified Mg-MOF-74: synthesis, characterization and CO_2 adsorption performance, *Environ. Eng. Res.* 28 (1) (2023) 210569.
[54] Z.Y. Gao, L. Liang, X. Zhang, P. Xu, J.M. Sun, Facile one-pot synthesis of Zn/Mg-MOF-74 with unsaturated coordination metal centers for efficient CO_2 adsorption and conversion to cyclic carbonates, *ACS Appl. Mater. Interfaces* 13 (51) (2021) 61334–61345.
[55] L.H. Wee, S. Vandenbrande, S.M.J. Rogge, J. Wieme, K. Asselman, E.O. Jardim, J. Silvestre-Albero, J.A.R. Navarro, V. van Speybroeck, J.A. Martens, C.E.A. Kirschhock, Chlorination of a zeolitic-imidazolate framework tunes packing and van der Waals interaction of carbon dioxide for optimized adsorptive separation, *J. Am. Chem. Soc.* 143 (13) (2021) 4962–4968.
[56] L. Lei, Y. Cheng, C.W. Chen, M. Kosari, Z.Y. Jiang, C. He, Taming structure and modulating carbon dioxide (CO_2) adsorption isosteric heat of nickel-based metal organic framework (MOF-74(Ni)) for remarkable CO_2 capture, *J. Colloid Interface Sci.* 612 (2022) 132–145.
[57] S.J. Chen, X.J. Li, J. Duan, Y. Fu, Z.Y. Wang, M. Zhu, N. Li, Investigation of highly efficient adsorbent based on Ni-MOF-74 in the separation of CO_2 from natural gas, *Chem. Eng. J.* 419 (2021) 129653.
[58] Y.H. Yang, L. Jin, L.P. Zhou, X.Z. Du, A molecular study of humid CO_2 adsorption capacity by Mg-MOF-74 surfaces with ligand functionalization, *Comput. Mater. Sci.* 209 (2022) 111407.
[59] J. Li, C.M. Zhu, Z. Qiao, X.Q. Chen, W. Wei, H.F. Ji, K. Sohlberg, A first principles study of interactions of CO_2 with surfaces of a Cu(benzene-1,3,5-tricarboxylate) metal organic framework, *Appl. Surf. Sci.* 385 (2016) 578–586.
[60] S. Kouser, A. Hezam, M.J.N. Khadri, S.A. Khanum, A review on zeolite imidazole frameworks: synthesis, properties, and applications, *J. Porous Mater.* 29 (3) (2022) 663–681.
[61] H. Wu, J.M. Simmons, G. Srinivas, W. Zhou, T. Yildirim, Adsorption sites and binding nature of CO_2 in prototypical metal–organic frameworks: a combined neutron diffraction and first-principles study, *J. Phys. Chem. Lett.* 1 (13) (2010) 1946–1951.
[62] B.Y. Liu, X. Chen, N. Huang, S.X. Liu, Y. Wang, X.C. Lan, F. Wei, T.F. Wang, Imaging the dynamic influence of functional groups on metal–organic frameworks, *Nat. Commun.* 14 (1) (2023) 4835.
[63] N. Planas, A.L. Dzubak, R. Poloni, L.C. Lin, A. McManus, T.M. McDonald, J.B. Neaton, J.R. Long, B. Smit, L. Gagliardi, The mechanism of carbon dioxide adsorption in an alkylamine-functionalized metal–organic framework, *J. Am. Chem. Soc.* 135 (20) (2013) 7402–7405.
[64] H. Wu, Y.S. Chua, V. Krungleviciute, M. Tyagi, P. Chen, T. Yildirim, W. Zhou, Unusual and highly tunable missing-linker defects in zirconium metal–organic framework UiO-66 and their important effects on gas adsorption, *J. Am. Chem. Soc.* 135 (28) (2013) 10525–10532.
[65] G.A. González-Martínez, J.A. Zárate, A. Martínez, E. Sánchez-González, J.R. Álvarez, E. Lima, E. González-Zamora, I.A. Ibarra, Confinement of alcohols to enhance CO_2 capture in MIL-53(Al), *RSC Adv.* 7 (40) (2017) 24833–24840.
[66] S. Mahajan, M. Lahtinen, Recent progress in metal–organic frameworks (MOFs) for CO_2 capture at different pressures, *J. Environ. Chem. Eng.* 10 (6) (2022) 108930.
[67] X.Q. Kong, E. Scott, W. Ding, J.A. Mason, J.R. Long, J.A. Reimer, CO_2 dynamics in a metal–organic framework with open metal sites, *J. Am. Chem. Soc.* 134 (35) (2012) 14341–14344.
[68] R.A. Maia, B. Louis, W.L. Gao, Q. Wang, CO_2 adsorption mechanisms on MOFs: a case study of open metal sites, ultra-microporosity and flexible framework, *React. Chem. Eng.* 6 (7) (2021) 1118–1133.
[69] H. Lyu, O.I. Chen, N. Hanikel, M.I. Hossain, R.W. Flaig, X.K. Pei, A. Amin, M.D. Doherty, R.K. Impastato, T.G. Glover, D.R. Moore, O.M. Yaghi, Carbon dioxide capture chemistry of amino acid functionalized metal–organic frameworks in humid flue gas, *J. Am. Chem. Soc.* 144 (5) (2022) 2387–2396.
[70] H.J. Zhu, W.J. Xue, H.L. Huang, L.Y. Chen, H.Y. Liu, C.L. Zhong, Water boosted CO_2/C_2H_2 separation in L-arginine functionalized metal: organic framework, *Nano Res.* 16 (5) (2023) 6113–6119.
[71] D. Tassé, V. Quezada-Novoa, C. Copeman, A.J. Howarth, A. Rochefort, Identification of adsorption sites for CO_2 in a series of rare-earth and Zr-based metal–organic frameworks, *ChemPhysChem* 26 (10) (2025) e202401050.
[72] H.L. Huang, W.J. Zhang, F. Yang, B. Wang, Q.Y. Yang, Y.B. Xie, C.L. Zhong, J.R. Li, Enhancing CO_2 adsorption and separation ability of Zr(IV)-based metal–organic frameworks through ligand functionalization under the guidance of the quantitative structure–property relationship model, *Chem. Eng. J.* 289 (2016) 247–253.
[73] R. Oktavian, R. Schireman, L.T. Glasby, G.M. Huang, F. Zanca, D. Fairen-Jimenez, M.T. Ruggiero, P.Z. Moghadam, Computational characterization of Zr-oxide MOFs for adsorption applications, *ACS Appl. Mater. Interfaces* 14 (51) (2022) 56938–56947.
[74] S.Y. Cai, J.S. Song, E.G. Huo, L. Zhang, X.D. Liu, Y.P. Chen, Microscopic insights on CO_2/N_2 separation in functionalized MOFs from molecular dynamics simulations and density functional theory calculation, *Chem. Eng. Sci.* 310 (2025) 121539.
[75] J.S. Song, L. Liu, S.Y. Cai, L. Shi, Molecular dynamics simulations of interfacial resistance of gases transport through MOF HKUST-1, *Chem. Eng. Sci.* 294 (2024) 120102.
[76] K.M. Jablonka, D. Ongari, S.M. Moosavi, B. Smit, Big-data science in porous materials: materials genomics and machine learning, *Chem. Rev.* 120 (16) (2020) 8066–8129.
[77] J.F. Li, Y. Li, Y.Z. Situ, Y.F. Wu, W.F. Wang, L.Q. Huang, C.Z. Cai, X.S. Huang, Y. F. Guan, S.X. Zhang, H.G. Li, L. Li, Y. Zhao, H. Liang, Z.W. Qiao, Unraveling the separation mechanism of gas mixtures in MOFs by combining the breakthrough curve with machine learning and high-throughput calculation, *Chem. Eng. Sci.* 299 (2024) 120470.
[78] J. Campbell, B. Tokay, Controlling the size and shape of Mg-MOF-74 crystals to optimise film synthesis on alumina substrates, *Microporous Mesoporous Mater.* 251 (2017) 190–199.
[79] N. Yang, T. Zhao, X. Wang, J.K. Gao, Green and facile synthesis of OH^- functionalized UiO-66 with controlled particle sizes to improve the selective separation of CO_2/N_2, *J. Solid State Chem.* 333 (2024) 124631.
[80] T. Li, J.E. Sullivan, N.L. Rosi, Design and preparation of a core–shell metal–organic framework for selective CO_2 capture, *J. Am. Chem. Soc.* 135 (27) (2013) 9984–9987.
[81] L.T. Du, Z.Y. Lu, K.Y. Zheng, J.Y. Wang, X. Zheng, Y. Pan, X.Z. You, J.F. Bai, Fine-tuning pore size by shifting coordination sites of ligands and surface polarization of metal–organic frameworks to sharply enhance the selectivity for CO_2, *J. Am. Chem. Soc.* 135 (2) (2013) 562–565.
[82] X.R. Shi, M. Qiao, Y. Wei, L.X. Yun, J.X. Wang, J.F. Chen, Green, efficient and controllable synthesis of high-quality MOF-74 with high gravity technology, *Green Chem.* 26 (10) (2024) 6209–6218.
[83] L. Bastin, P.S. Bárcia, E.J. Hurtado, J.A.C. Silva, A.E. Rodrigues, B.L. Chen, A microporous metal–organic framework for separation of CO_2/N_2 and CO_2/CH_4 by fixed-bed adsorption, *J. Phys. Chem. C* 112 (5) (2008) 1575–1581.
[84] J. An, N.L. Rosi, Tuning MOF CO_2 adsorption properties *via* cation exchange, *J. Am. Chem. Soc.* 132 (16) (2010) 5578–5579.
[85] M. Witman, S.L. Ling, S. Anderson, L.H. Tong, K.C. Stylianou, B. Slater, B. Smit, M. Haranczyk, In silico design and screening of hypothetical MOF-74 analogs and their experimental synthesis, *Chem. Sci.* 7 (9) (2016) 6263–6272.
[86] G.E. Cmarik, M. Kim, S.M. Cohen, K.S. Walton, Tuning the adsorption properties of UiO-66 *via* ligand functionalization, *Langmuir* 28 (44) (2012) 15606–15613.
[87] B. Soleimani, M. Niknam Shahrak, K.S. Walton, The influence of different functional groups on enhancing CO_2 capture in metal–organic framework adsorbents, *J. Taiwan Inst. Chem. Eng.* 163 (2024) 105638.
[88] S. Norouzbahari, Z.M. Lighvan, A. Ghadimi, B. Sadatnia, ZIF-8@Zn-MOF-74 core–shell metal–organic framework (MOF) with open metal sites: synthesis, characterization, and gas adsorption performance, *Fuel* 339 (2023) 127463.
[89] H.R. Abid, Z.H. Rada, L.H. Liu, S.B. Wang, S.M. Liu, Striking CO_2 capture and CO_2/N_2 separation by Mn/Al bimetallic MIL-53, *Polyhedron* 193 (2021) 114898.
[90] M. Zhang, J.S. Zhou, X.L. Guo, X.K. Zeng, L. Shi, T.T. Zhang, Y.F. He, X.T. Zhou, S.Y. Shan, K.L. Yao, Amine-functionalized MIL-101 sorbents modified with alkali metal cations for enhanced CO_2 capture and electroreduction conversion, *Chem. Eng. J.* 515 (2025) 163668.
[91] K.N. Song, S.J. Liang, X.H. Zhong, M.Y. Wang, X.F. Mo, X.Q. Lei, Z. Lin, Tailoring the crystal forms of the Ni-MOF catalysts for enhanced photocatalytic CO_2-to-CO performance, *Appl. Catal. B Environ.* 309 (2022) 121232.
[92] A. Kazemi, M.A. Pordsari, M. Tamtaji, F. Zainali, S. Keshavarz, H. Baesmat, F. Manteghi, A. Ghaemi, S. Rohani, W.A. Goddard III, Eco-friendly synthesis and morphology control of MOF-74 for exceptional CO_2 capture performance with DFT validation, *Sep. Purif. Technol.* 361 (2025) 131328.
[93] M.I. Hossain, J.D. Cunningham, T.M. Becker, B.E. Grabicka, K.S. Walton, B.D. Rabideau, T.G. Glover, Impact of MOF defects on the binary adsorption of CO_2 and water in UiO-66, *Chem. Eng. Sci.* 203 (2019) 346–357.
[94] J.B. Niu, H. Li, L.G. Tao, Q. Fan, W. Liu, M.C. Tan, Defect engineering of low-coordinated metal–organic frameworks (MOFs) for improved CO_2 access and capture, *ACS Appl. Mater. Interfaces* 15 (26) (2023) 31664–31674.
[95] G.H. Zhang, S.C. Mo, H.T. Xu, X.Y. Yan, B.L. Dou, G.M. Cui, Q.G. Yang, W. Lu, Enhanced CO_2 adsorption performance by crystal defect method of multi-level pore Mg-MOF-74 using organic acids, *Gas Sci. Eng.* 120 (2023) 205162.
[96] R. Hardian, S. Dissegna, A. Ullrich, P.L. Llewellyn, M.V. Coulet, R.A. Fischer, Tuning the properties of MOF-808 *via* defect engineering and metal nanoparticle encapsulation, *Chemistry* 27 (22) (2021) 6804–6814.
[97] Y. Fu, Y.F. Yao, A.C. Forse, J.H. Li, K. Mochizuki, J.R. Long, J.A. Reimer, G. de Paëpe, X.Q. Kong, Solvent-derived defects suppress adsorption in MOF-74, *Nat. Commun.* 14 (1) (2023) 2386.
[98] Y. Cao, Y.X. Zhao, Z.J. Lv, F.J. Song, Q. Zhong, Preparation and enhanced CO_2 adsorption capacity of UiO-66/graphene oxide composites, *J. Ind. Eng. Chem.* 27 (2015) 102–107.

[99] S.S. Shang, Z.Y. Tao, C. Yang, A. Hanif, L.C. Li, D.C.W. Tsang, Q.F. Gu, J. Shang, Facile synthesis of CuBTC and its graphene oxide composites as efficient adsorbents for CO_2 capture, *Chem. Eng. J.* 393 (2020) 124666.

[100] Z. Haeri, B. Ramezanzadeh, M. Ramezanzadeh, Recent progress on the metal–organic frameworks decorated graphene oxide (MOFs-GO) nano-building application for epoxy coating mechanical-thermal/flame-retardant and anti-corrosion features improvement, *Prog. Org. Coating* 163 (2022) 106645.

[101] Y.W. Chen, D.F. Lv, J.L. Wu, J. Xiao, H.X. Xi, Q.B. Xia, Z. Li, A new MOF-505@GO composite with high selectivity for CO_2/CH_4 and CO_2/N_2 separation, *Chem. Eng. J.* 308 (2017) 1065–1072.

[102] A. Policicchio, Y.X. Zhao, Q. Zhong, R.G. Agostino, T.J. Bandosz, Cu-BTC/aminated graphite oxide composites as high-efficiency CO_2 capture media, *ACS Appl. Mater. Interfaces* 6 (1) (2014) 101–108.

[103] P. Choudhary, S.K. Ola, I. Chopra, V. Dhayal, D.S. Shekhawat, Metal–organic framework (MOF)/graphene–oxide (GO) nanocomposites materials: a potential formulation for anti-corrosive coatings—a review, *Mater. Today Proc.* 79 (2023) 172–178.

[104] A. Sathiyaseelan, X. Zhang, Y.T. Lu, N.A. Azeez, L.N. Zhang, G.S. Krishnakumar, M.H. Wang, Exploring the synthesis, properties, and potential of chitosan-functionalized metal–organic frameworks in emerging applications, *Prog. Mater. Sci.* 148 (2025) 101387.

[105] N. Hammi, M. Bonneau, A. El Kadib, S. Kitagawa, T. Loiseau, C. Volkringer, S. Royer, J. Dhainaut, Enhanced gas adsorption in HKUST-1@chitosan aerogels, cryogels, and xerogels: an evaluation study, *ACS Appl. Mater. Interfaces* 15 (46) (2023) 53395–53404.

[106] N. Noorani, A. Mehrdad, Impregnation of amine functionalized deep eutectic solvents in NH_2-MIL-53(Al) MOF for CO_2/N_2 separation, *Sci. Rep.* 13 (1) (2023) 13012.

[107] M. Teixeira, R.A. Maia, S. Shanmugam, B. Louis, S.A. Baudron, Impact of urea-based deep eutectic solvents on Mg-MOF-74 morphology and sorption properties, *Microporous Mesoporous Mater.* 343 (2022) 112148.

[108] C. Zhang, T.Y. Su, X.Q. Zhang, D.Y. Zhang, T. Xuan, L.W. Wang, Porous core-membrane microstructured nanomaterial composed of deep eutectic solvents and MOF-808 for CO_2 capture, *ChemSusChem* 16 (24) (2023) e202300864.

[109] D.Y. Zhang, C. Zhang, X.Q. Zhang, Y.Q. Tian, X.S. Cheng, X.C. Zhu, L.W. Wang, Efficient low-pressure CO_2 capture *via* ZIF-8 modified by deep eutectic solvents, *Sep. Purif. Technol.* 353 (2025) 128359.

[110] N. Noorani, A. Mehrdad, Improving the separation of CO_2/N_2 using impregnation of a deep eutectic solvent on a porous MOF, *ACS Omega* 9 (8) (2024) 9516–9525.

[111] N. Vrtovec, S. Jurjevec, N. Zabukovec Logar, M. Mazaj, S. Kovačič, Metal oxide-derived MOF-74 polymer composites through Pickering emulsion-templating: interfacial recrystallization, hierarchical architectures, and CO_2 capture performances, *ACS Appl. Mater. Interfaces* 15 (14) (2023) 18354–18361.

[112] X.Y. Liu, Q. Zhang, H. Zhu, S.P. Zhu, Hierarchically porous SIFSIX-3-Ni/PAN composite beads for carbon dioxide adsorption, *Macromol. Mater. Eng.* 308 (11) (2023) 2300173.

[113] J. Park, Y.S. Chae, D.W. Kang, M. Kang, J.H. Choe, S. Kim, J.Y. Kim, Y.W. Jeong, C.S. Hong, Shaping of a metal–organic framework-polymer composite and its CO_2 adsorption performances from humid indoor air, *ACS Appl. Mater. Interfaces* 13 (21) (2021) 25421–25427.

[114] S. Basu, A. Cano-Odena, I.F.J. Vankelecom, Asymmetric Matrimid®/$[Cu_3(BTC)_2]$ mixed-matrix membranes for gas separations, *J. Membr. Sci.* 362 (1–2) (2010) 478–487.

[115] T. Li, Y.C. Pan, K.V. Peinemann, Z.P. Lai, Carbon dioxide selective mixed matrix composite membrane containing ZIF-7 nano-fillers, *J. Membr. Sci.* 425 (2013) 235–242.

[116] L. Ge, W. Zhou, V. Rudolph, Z.H. Zhu, Mixed matrix membranes incorporated with size-reduced Cu-BTC for improved gas separation, *J. Mater. Chem. A* 1 (21) (2013) 6350–6358.

[117] M.S. Rostami, M.M. Khodaei, Effect of incorporated hybrid MIL-53(Al) and MWCNT into PES membrane for CO_2/CH_4 and CO_2/N_2 separation, *Fuel* 356 (2024) 129598.

[118] J.J. Sun, Q.Q. Li, G.N. Chen, J.G. Duan, G.P. Liu, W.Q. Jin, MOF-801 incorporated PEBA mixed-matrix composite membranes for CO_2 capture, *Sep. Purif. Technol.* 217 (2019) 229–239.

[119] X.R. Zhang, X.F. Ren, Y.H. Wang, J.P. Li, ZIF-8@NENP-NH_2 embedded mixed matrix composite membranes utilized as CO_2 capture, *Sep. Purif. Technol.* 303 (2022) 122195.

[120] Y.J. Chang, L. Wang, Z.F. Jiang, R. Zhang, H.J. Zhu, D.E. Zhang, J. Zhu, X. Kong, H. L. Huang, Zwitterionic metal–organic framework with highly dispersed ionic liquid for enhancing CO_2 capture, *Sep. Purif. Technol.* 326 (2023) 124828.

[121] X.Q. Li, K. Chen, R.L. Guo, Z. Wei, Ionic liquids functionalized MOFs for adsorption, *Chem. Rev.* 123 (16) (2023) 10432–10467.

[122] C.L. Zhao, X.Y. Li, G.N. Liu, X.Z. Wang, Selective adsorption of trace CO_2 by immobilized amino acid ionic liquids with ultra-micropores based on amino MOFs, *Sep. Purif. Technol.* 356 (2025) 129742.

[123] Q. Al-Naddaf, A.A. Rownaghi, F. Rezaei, Multicomponent adsorptive separation of CO_2, CO, CH_4, N_2, and H_2 over core-shell zeolite-5A@MOF-74 composite adsorbents, *Chem. Eng. J.* 384 (2020) 123251.

[124] S.M. Cui, Y.J. Shao, W.Q. Zhong, Molecular sieves hybrid metal–organic framework for efficient simultaneously capturing carbon dioxide and collecting water from air, *Chem. Eng. J.* 499 (2024) 155912.

[125] F. Feyzbar-Khalkhali-Nejad, S.M. Taghavi Kouzehkanan, E. Hassani, B. Hassani, H. Jahromi, S. Adhikari, T.S. Oh, ZSM-5@MOF-199 core-shell composite adsorbent: rapid ambient synthesis and CO/CO_2 adsorption, *Chem. Eng. Sci.* 292 (2024) 119969.

[126] J.J. Wang, L.Z. Wang, Y. Wang, F. Yang, J.W. Li, X.Y. Guan, J.J. Zong, F. Zhou, J. H. Huang, Y.N. Liu, Covalently connected core–shell NH_2-UiO-66@Br-COFs hybrid materials for CO_2 capture and I_2 vapor adsorption, *Chem. Eng. J.* 438 (2022) 135555.

[127] C. Chen, Y.K. Zhang, C.J. Hu, Z.W. Jiang, J. Ma, Scalable upgrading metal–organic frameworks through ambient and controllable electron-beam irradiation for CO_2 capture and conversion, *Sep. Purif. Technol.* 363 (2025) 132270.

[128] L. Valenzano, B. Civalleri, S. Chavan, G.T. Palomino, C.O. Areán, S. Bordiga, Computational and experimental studies on the adsorption of CO, N_2, and CO_2 on Mg-MOF-74, *J. Phys. Chem. C* 114 (25) (2010) 11185–11191.

[129] W.M. Bloch, R. Babarao, M.R. Hill, C.J. Doonan, C.J. Sumby, Post-synthetic structural processing in a metal–organic framework material as a mechanism for exceptional CO_2/N_2 selectivity, *J. Am. Chem. Soc.* 135 (28) (2013) 10441–10448.

[130] J.H. Kim, S.H. So, M. Kim, E. Choi, N. Lee, K. Eum, Y.H. Kim, D.W. Kim, ZIF-8/graphene nanoribbon hybrid nanoplates for mixed-matrix membranes with enhanced CO_2 separation performance, *J. Membr. Sci.* 720 (2025) 123805.

[131] C.L. Jiao, Z.D. Li, X.X. Li, M. Wu, H.Q. Jiang, Improved CO_2/N_2 separation performance of Pebax composite membrane containing polyethyleneimine functionalized ZIF-8, *Sep. Purif. Technol.* 259 (2021) 118190.

[132] P. Sardar, R. Manna, G. Bhattacharya, S. Raj, S. Yadav, S. Rahut, S. Upadhyayula, A.N. Samanta, Enhanced CO_2 adsorption efficiency through aminoethylethanolamine functionalized porous ZIF-8 nanoparticles: experimental investigations, isotherm and RSM modeling, *Sep. Purif. Technol.* 360 (2025) 131090.

[133] S.K. Xian, F. Xu, C. Ma, Y. Wu, Q.B. Xia, H.H. Wang, Z. Li, Vapor-enhanced CO_2 adsorption mechanism of composite PEI@ZIF-8 modified by polyethyleneimine for CO_2/N_2 separation, *Chem. Eng. J.* 280 (2015) 363–369.

[134] A. Mohammadi, A. Nakhaei Pour, Triethylenetetramine-impregnated ZIF-8 nanoparticles for CO_2 adsorption, *J. CO_2 Util.* 69 (2023) 102424.

[135] Z.J. Zhang, S.K. Xian, Q.B. Xia, H.H. Wang, Z. Li, J. Li, Enhancement of CO_2 adsorption and CO_2/N_2 selectivity on ZIF-8 *via* postsynthetic modification, *AIChE J.* 59 (6) (2013) 2195–2206.

[136] J.J. Zhang, G.Y. Li, S.B. Zhang, J.G. Shao, X. Zhang, S.H. Zhang, H.P. Yang, H.P. Chen, Controlled synthesis of biochar with flower-like morphology for CO_2 adsorption: enrichment and efficient accessibility of N-containing sites, *ACS Appl. Mater. Interfaces* 17 (4) (2025) 6742–6754.

[137] G. Lee, S.H. Jhung, Obtaining both high CO_2 adsorption capacity and CO_2/N_2 selectivity *via* blocking N_2 adsorption sites by grafting bulky diamine on metal–organic framework, *Fuel* 394 (2025) 135143.

[138] V. Rahmanian, S. Razavi, M.O. Abdelmigeed, M.Z. Ahmad Ebrahim, G.N. Parsons, F.X. Li, T. Pirzada, S.A. Khan, Metal organic framework impregnated nanofibrous aerogels: a 3D structured matrix for CO_2 capture, *ACS Appl. Mater. Interfaces* 17 (17) (2025) 25623–25633.

[139] Y.Q. Zhou, Y. Yuan, X.L. Liu, Z. Wang, Highly permeable MOF NH_2-MIL-101(Cr) fragment membranes for CO_2/N_2 separation, *J. Membr. Sci.* 722 (2025) 123918.

[140] Z.K. Liu, H.F. Zhao, B.Q. Hua, Y. Wang, T.Y. Lu, M. Guo, G.Y. Dong, J.Y. Zhu, Y. T. Zhang, Ionic liquid-functionalized defective MOFs for membrane-based CO_2 separation: a dual optimization approach for interface and transport, *ACS Appl. Mater. Interfaces* 17 (4) (2025) 6867–6877.

[141] S. Fakhraie, H.R. Rajabi, E. Ghasemy, A. Rashidi, Y. Orooji, M.H. Hadizadeh, D. Maklavany, Exceptional CO_2 and H_2S adsorption by tuning micro/mesopore ratios with embedded graphene oxide/N-doped carbon quantum dots in MIL-101(Cr): experimental and computational insights, *J. Colloid Interface Sci.* 683 (Pt 2) (2025) 769–783.

[142] C.N. Li, Z.P. Tao, L. Liu, D.Q. Yuan, Z.B. Han, Cation exchange strategy of ellagic acid-based microporous metal–organic framework for efficient CO_2/N_2 and CO_2/CH_4 separation, *Chem. Eng. J.* 502 (2024) 157956.

[143] H.J. Zhao, Y. Jiang, T.T. Zhang, H. Wang, S.J. Chen, G.D. Zhao, A fluoride-rich metal–organic framework for efficient CO_2 capture under humid conditions, *Fuel* 381 (2025) 133553.

[144] F. Yang, X.C. Zhu, J.Y. Wu, R.Z. Wang, T.S. Ge, Kinetics and mechanism analysis of CO_2 adsorption on LiX@ZIF-8 with core shell structure, *Powder Technol.* 399 (2022) 117090.

[145] Y.J. Wan, D.K. Kong, F. Xiong, T.J. Qiu, S. Gao, Q.N. Zhang, Y.F. Miao, M.L. Qin, S.Q. Wu, Y.G. Wang, R.Q. Zhong, R.Q. Zou, Enhancing hydrophobicity *via* core–shell metal organic frameworks for high-humidity flue gas CO_2 capture, *Chin. J. Chem. Eng.* 61 (2023) 82–89.

[146] F. Yang, J.Y. Wu, X.C. Zhu, T.S. Ge, R.Z. Wang, Enhanced stability and hydrophobicity of LiX@ZIF-8 composite synthesized environmental friendly for CO_2 capture in highly humid flue gas, *Chem. Eng. J.* 410 (2021) 128322.

[147] J.M. Yu, P.B. Balbuena, How impurities affect CO_2 capture in metal–organic frameworks modified with different functional groups, *ACS Sustainable Chem. Eng.* 3 (1) (2015) 117–124.

[148] M.M. Jin, Y.X. Li, C. Gu, X.Q. Liu, L.B. Sun, Tailoring microenvironment of adsorbents to achieve excellent CO_2 uptakes from wet gases, *AIChE J.* 66 (11) (2020) e16645.
[149] S.K. Xian, J.J. Peng, Z.J. Zhang, Q.B. Xia, H.H. Wang, Z. Li, Highly enhanced and weakened adsorption properties of two MOFs by water vapor for separation of CO_2/CH_4 and CO_2/N_2 binary mixtures, *Chem. Eng. J.* 270 (2015) 385–392.
[150] J.H. Choe, H. Kim, M. Kang, H. Yun, S.Y. Kim, S.M. Lee, C.S. Hong, Functionalization of diamine-appended MOF-based adsorbents by ring opening of epoxide: long-term stability and CO_2 recyclability under humid conditions, *J. Am. Chem. Soc.* 144 (23) (2022) 10309–10319.
[151] O.I. Chen, C.H. Liu, K.Y. Wang, E. Borrego-Marin, H.Z. Li, A.H. Alawadhi, J.A.R. Navarro, O.M. Yaghi, Water-enhanced direct air capture of carbon dioxide in metal–organic frameworks, *J. Am. Chem. Soc.* 146 (4) (2024) 2835–2844.
[152] S. Ullah, M.A. Bustam, M.A. Assiri, A.G. Al-Sehemi, F.A. Abdul Kareem, A. Mukhtar, M. Ayoub, G. Gonfa, Synthesis and characterization of iso-reticular metal–organic framework-3 (IRMOF-3) for CO_2/CH_4 adsorption: impact of post-synthetic aminomethyl propanol (AMP) functionalization, *J. Nat. Gas Sci. Eng.* 72 (2019) 103014.
[153] S. Ullah, M.A. Bustam, M.A. Assiri, A.G. Al-Sehemi, M. Sagir, F.A. Abdul Kareem, A.E.I. Elkhalifah, A. Mukhtar, G. Gonfa, Synthesis, and characterization of metal–organic frameworks-177 for static and dynamic adsorption behavior of CO_2 and CH_4, *Microporous Mesoporous Mater.* 288 (2019) 109569.
[154] M.K. Taylor, T. Runčevski, J. Oktawiec, J.E. Bachman, R.L. Siegelman, H. Jiang, J.A. Mason, J.D. Tarver, J.R. Long, Near-perfect CO_2/CH_4 selectivity achieved through reversible guest templating in the flexible metal–organic framework Co(bdp), *J. Am. Chem. Soc.* 140 (32) (2018) 10324–10331.
[155] Z.L. Zheng, A.H. Alawadhi, O.M. Yaghi, Green synthesis and scale-up of MOFs for water harvesting from air, *Mol. Front. J.* 7 (01n02) (2023) 20–39.
[156] Y. Wang, T.F. He, J.G. Cao, K. Li, C.Q. Wang, Q. Liu, Y. Zhang, Waste-to-microporous framework: Al/Si fractionation of coal fly ash coupled with waste PET conversion for separated synthesis of high-porosity MIL-53(Al) and ZSM-5 toward efficient dyes and CO_2 capture, *J. Mol. Struct.* 1335 (2025) 141984.
[157] A. Deacon, L. Briquet, M. Malankowska, F. Massingberd-Mundy, S. Rudić, T. L. Hyde, H. Cavaye, J. Coronas, S. Poulston, T. Johnson, Understanding the ZIF-L to ZIF-8 transformation from fundamentals to fully costed kilogram-scale production, *Commun. Chem.* 5 (1) (2022) 18.
[158] J.L. Woodliffe, J. Molinar-Díaz, B. Holland, O.H. Hussein, E. Lester, K. Robertson, Magnetic framework composites *via* continuous flow syntheses for CO_2 capture, *Chem. Eng. J.* 503 (2025) 158445.
[159] W.T. Han, M.H. Shi, H.L. Jiang, Scalable and low-energy synthesis of metal–organic frameworks by a seed-mediated approach, *Angew. Chem. Int. Ed.* 64 (13) (2025) e202421942.
[160] Editorial, A market for metal–organic frameworks, *Nat. Mater.* 24 (2) (2025) 157.